PARAMETRIC INSTABILITIES IN THE DISCRETE SINE-GORDON EQUATION

by

C.G. Goedde, A.J. Lichtenberg, and M.A. Lieberman

Memorandum No. UCB/ERL M89/79

10 July 1989

COVER PAGE

PARAMETRIC INSTABILITIES IN THE DISCRETE SINE-GORDON EQUATION

by

C.G. Goedde, A.J. Lichtenberg, and M.A. Lieberman

Memorandum No. UCB/ERL M89/79

10 July 1989

ELECTRONICS RESEARCH LABORATORY

College of Engineering
University of California, Berkeley
94720

TITLE PAGE

PARAMETRIC INSTABILITIES IN THE DISCRETE SINE-GORDON EQUATION

by

C.G. Goedde, A.J. Lichtenberg, and M.A. Lieberman

Memorandum No. UCB/ERL M89/79

10 July 1989

ELECTRONICS RESEARCH LABORATORY

College of Engineering
University of California, Berkeley
94720

Parametric Instabilities in the Discrete Sine-Gordon Equation

C. G. Goedde

Department of Physics

University of California, Berkeley, CA 94720

A. J. Lichtenberg and **M. A. Lieberman**

Department of Electrical Engineering and Computer Sciences

and the Electronics Research Laboratory

University of California, Berkeley, CA 94720

ABSTRACT

The one-dimensional Sine-Gordon equation is an example of an exactly solvable nonlinear partial differential equation. When discretized on a periodic lattice in space and in time, it corresponds to a lattice of pendula coupled by linear springs. We show that the discretized system is unstable to a parametric mode when the frequency of time discretization is sufficiently small, and we obtain the instability condition and growth rate. By considering the effects of two finite amplitude modes, we also obtain the nonlinear saturation of the instability. We also examine how solutions of the exact Sine-Gordon equation behave under this map, both in and away from the parametrically unstable regime.

1. Introduction

There has been considerable interest in understanding the dynamical behavior of systems with many degrees of freedom. One question is whether the intrinsic stochasticity which appears in two degrees of freedom [1] tends to increasingly fill the phase space volume as the number of degrees of freedom increase. A related question is the effect of discretizing a nonlinear partial differential equation whose continuous solution is integrable. What happens to any stochasticity in the discrete system as the discretization becomes finer and finer?

One of the earliest attempts to observe the behavior of a discretized nonlinear partial differential equation was made by Fermi, Pasta, and Ulam [2] who numerically examined the discretization of the equation

$$\frac{\partial^2 x}{\partial t^2} - \frac{\partial^2 x}{\partial z^2}\left[1 + 3\beta\left(\frac{\partial x}{\partial z}\right)^2\right] = 0,$$

which corresponds to a set of equimass particles connected by nonlinear springs. The original result with 64 particles indicated that at low energy equipartition was not obtained among the oscillators, but rather a beat phenomenon existed with regular approximate recurrences of initial conditions. This result, contrary to the original expectation of equipartition, stimulated a number of investigations [3–5]. It was found that transitions could occur with increasing energy from apparently regular to apparently irregular motion. These observations are consistent with the understanding of coupled systems of a few dimensions in which such transitions occur when resonances between degrees of freedom overlap in the action space [1]. In fact, Izrailev and Chirikov [5], using a normal mode expansion, developed an analytic criterion which roughly predicted the numerical results. More recent work has attempted to characterize the transition to energy equipartition in terms of the energy density of the system [6–8].

These investigations suffered from the problem that analytic solutions to the original differential equation were not available, to compare to the discretized results. Since those studies, a class of partial differential equations have been studied for which solutions are available [9–11]. A particularly interesting one is the Sine-Gordon equation which, when discretized in space, corresponds to linearly coupled pendula. Additionally, discretizing in time results in coupled standard maps. The behavior of a single standard map has been extensively studied, with the transition, with increasing energy, from regular to stochastic motion well understood [1,12]. For coupled maps we know that an additional phenomenon of Arnold diffusion occurs, which allows diffusion of some initial conditions through large portions of the phase space for any initial system energy. With two coupled maps, at low energy, the fraction of the phase space that can participate in the diffusion and the rate of diffusion are both small [1,12]. It is not known, however, how these quantities scale as the number of coupled maps (the number of dimensions) increases.

It is the purpose of this paper to investigate some aspects of high dimensional systems by discretizing the Sine-Gordon equation in space and time. Of particular interest is the effect of resonances between the time and space periodicities, which lead to parametric instabilities for certain values of the system parameters.

2. Basic Formulation

We begin by considering the one-dimensional unperturbed Sine-Gordon equation

$$\phi_{tt} - \phi_{xx} + \sin\phi = 0, \tag{1}$$

and make the space coordinate discrete through the substitutions

$$\begin{aligned}
\phi(x,t) &\longrightarrow \phi_j(t) \qquad j = 1, \ldots, N, \\
\phi_x(x,t) &\longrightarrow \frac{\phi_{j+1}(t) - \phi_j(t)}{\Delta x}, \\
\phi_{xx}(x,t) &\longrightarrow \frac{(\phi_{j+1}(t) - \phi_j(t)) + (\phi_{j-1}(t) - \phi_j(t))}{(\Delta x)^2}.
\end{aligned}$$

We also consider a periodic domain of length L, so that $\phi_{j+N} = \phi_j$, and the spacing between oscillators, Δx, is L/N. Note that since the formulation of (1) is dimensionless, these lengths, as well as all other physical quantities, such as energy and frequency, are dimensionless. With the change of notation $\phi_j = q_j$, $\dot{\phi}_j = p_j$, we can write the discretized Hamiltonian for the system

$$H = \sum_{i=1}^{N} \frac{1}{2} p_i^2 + \sum_{i=1}^{N} \Gamma^2 (1 - \cos q_i) + \sum_{i,j=1}^{N} A_{ij} q_i q_j, \tag{2}$$

where the coupling matrix A_{ij} is given by

$$A_{ij} = \frac{(2\delta_{i,j} - \delta_{i,j+1} - \delta_{i,j-1})}{(\Delta x)^2},$$

where δ_{ij} is the Kronicker δ-function.

This Hamiltonian has the following interpretation: the first two terms correspond to N pendula, and the last term represents harmonic coupling between nearest neighbors. Here we have also introduced the parameter Γ, the linearized frequency of the pendula. Taking $\Gamma = 1$ corresponds to the discretized Sine-Gordon equation.

Since the linear part of this Hamiltonian (the first and third terms of (2)) is exactly solvable, it is useful to analyze the problem in terms of the normal modes of the harmonic springs. The eigenvectors of the linear system can be written as

$$e_{ir} = \frac{1}{\sqrt{N}}\left(\cos\frac{2\pi ir}{N} - \sin\frac{2\pi ir}{N}\right),$$

which are orthonormal: $\sum_{i=1}^{N} e_{ir}e_{is} = \delta_{rs}$. We define new variables, u and v, through

$$u_r = \sum_{i=1}^{N} q_i e_{ir}, \qquad v_r = \sum_{i=1}^{N} p_i e_{ir}, \tag{3a}$$

such that the q_i and p_i can be represented as

$$q_i = \sum_{r=1}^{N} u_r e_{ir}, \qquad p_i = \sum_{r=1}^{N} v_r e_{ir}. \tag{3b}$$

In terms of u and v the Hamiltonian becomes

$$H = \sum_{r=1}^{N}\left[\frac{v_r^2}{2} + \omega_r^2\frac{u_r^2}{2}\right] + \Gamma^2\sum_{i=1}^{N}\left[1 - \cos\left(\sum_{r=1}^{N} u_r e_{ir}\right)\right] = H_0 + H_1. \tag{4}$$

Thus we have a system of N harmonic oscillators, of frequencies $\omega_1 \ldots \omega_{N/2}$, coupled through the cosines. Since we have a finite number of oscillators, the spectrum is discrete, and the (dimensionless) frequencies are given by

$$\omega_r = \frac{2}{\Delta x}\sin\frac{\pi r}{N} = \frac{2N}{L}\sin\frac{\pi r}{N}.$$

Note that the maximum frequency is $\omega_{N/2} = 2N/L$, and the frequencies are pairwise degenerate: $\omega_r = \omega_{N-r}$. In this formulation it is convenient to think of the linear system as the fundamental system, and the nonlinearity as a perturbation, although we have not assumed that $H_1 \ll H_0$.

The equations of motion are given by

$$\dot{u}_s = \frac{\partial H}{\partial v_s} = v_s, \tag{5a}$$

$$\dot{v}_s = -\frac{\partial H}{\partial u_s} = -\omega_s^2 u_s - \Gamma^2 \sum_{i=1}^{N} e_{is} \sin\left(\sum_{r=1}^{N} u_r e_{ir}\right). \tag{5b}$$

The discretization has converted the an infinite dimensional system described by a partial differential equation to a $2N$ dimensional system described by a set of coupled ordinary differential equations.

The dynamical system can be conveniently investigated, numerically, by discretizing (5) in time as well as space, to obtain a mapping. This has the effect of adding an external drive to the system, which adds new physics: for example, energy is no longer conserved. We modify the Hamiltonian by multiplying H_1 in equation (4) by an infinite series of delta functions to obtain

$$H_1 = \Gamma^2 \left(\sum_{i=1}^{N}\left[1 - \cos\left(\sum_{r=1}^{N} u_r e_{ir}\right)\right]\right)\left(\sum_{m=-\infty}^{\infty} \delta(t/T - m)\right). \tag{6}$$

In the physical model this corresponds to pulsing gravity with period T. The equations of motion are then

$$\dot{u}_s = v_s, \tag{7a}$$

$$\dot{v}_s = -\omega_s^2 u_s - \Gamma^2 \left(\sum_{m=-\infty}^{\infty} \delta(t/T - m)\right) \sum_{i=1}^{N} e_{is} \sin\left(\sum_{r=1}^{N} u_r e_{ir}\right). \tag{7b}$$

The delta functions allow us to integrate this immediately through the boundary conditions at $t = mT$:

$$\begin{aligned} u_s' - u_s &= 0, \\ v_s' - v_s &= -\Gamma^2 T \sum_{i=1}^{N} e_{is} \sin\left(\sum_{r=1}^{N} u_r e_{ir}\right), \end{aligned} \tag{8}$$

Here the primed [unprimed] variables denote quantities just after [before] a gravity pulse. Physically the positions are unchanged by the gravity pulse and the momenta undergo an instantaneous change. The dynamics then evolve according to the area preserving map

$$u_s' = u_s \cos\omega_s T + \frac{1}{\omega_s}\left[v_s - \Gamma^2 T \sum_{i=1}^{N} e_{is} \sin\left(\sum_{r=1}^{N} u_r e_{ir}\right)\right] \sin\omega_s T, \tag{9a}$$

$$v_s' = -\omega_s u_s \sin\omega_s T + \left[v_s - \Gamma^2 T \sum_{i=1}^{N} e_{is} \sin\left(\sum_{r=1}^{N} u_r e_{ir}\right)\right] \cos\omega_s T, \tag{9b}$$

Note that when $s = N$, $\omega_N = 0$, and the quantity $\sin\omega_N T/\omega_N$ is replaced by T. Iterating this map gives the complete evolution of the discretized system in the $2N$ dimensional phase space.

It is well known that the unperturbed Sine-Gordon equation (1) can be solved by a Backlund transformation [10]. An example for an infinite spatial domain is the so-called Sine-Gordon breather:

$$\phi_B(x,t) = 4\tan^{-1}\frac{\alpha \sin\nu\gamma(t - t_0 - \beta x)}{\nu\cosh\alpha\gamma(x - x_0 - \beta t)},$$

where ν is the frequency of the breather, which has velocity β, $\gamma = 1/\sqrt{1-\beta^2}$ and $\alpha^2 + \nu^2 = 1$. This solution satisfies the boundary condition $\phi(x = \pm\infty) = 0$. If the x domain is periodic, with length L, the boundary conditions are

$$\phi(x = L/2, t) = \phi(x = -L/2, t), \tag{10a}$$

$$\phi_x(x = L/2, t) = \phi_x(x = -L/2, t). \tag{10b}$$

In this case the analogous solution is [11]

$$\phi(x,t) = 4\tan^{-1}\left(A\ \mathrm{cn}(\mu x, k_x)\mathrm{cn}(\nu t, k_t)\right), \tag{11}$$

where the cn are cosine-amplitude Jacobi elliptic functions. This satisfies the boundary condition (10a) identically, and (10b) sets the spatial periodicity of the breather through $\mu = 4mK/L$, m integer, where K is the quarter period of the elliptic functions:

$$K = \int_0^{\pi/2} \frac{d\theta}{\sqrt{1 - k_x^2 \sin^2\theta}}.$$

The other parameters in equation (11) are given by

$$\begin{aligned} \nu^2 - \mu^2 &= \frac{1-A^2}{1+A^2}, \\ k_x^2 &= \frac{A^2}{\mu^2(1+A^2)^2}\left(1 + \mu^2(1+A^2)\right), \\ k_t^2 &= \frac{A^2}{\nu^2(1+A^2)^2}\left(-1 + \nu^2(1+A^2)\right). \end{aligned}$$

The parameter k_t determines the frequency of oscillation of the breather (which we shall call ω_B) in the same way that k_x determines the spatial periodicity.

While equation (11) is an exact solution of (1), it will not be an exact solution of the set of maps (9). By investigating the conditions under which these solutions are stable, we hope to understand the effects of discreteness on the system. Thus we look at the decay of these solutions when put on a lattice and pulsed by gravity with period T. We consider a lattice with 256 oscillators, and compare the behavior of two initial conditions of the form (11) under the set of maps (9). The spatial domain is of length $L = 32$, giving a maximum linear frequency of $\omega_{N/2} = 16\sin(\pi/2) = 16.0$ and a minimum of $\omega_1 = 16\sin(\pi/N) \simeq 0.196$ (recall that the pendula have a linear frequency $\Gamma = 1$), and we use a time step $T = 0.1$. The initial configurations of two such solutions are shown in Figure 1, which are determined by the parameter values $k_x = \sqrt{0.9}$ and $k_x = \sqrt{1 - 10^{-6}}$, corresponding to breather-type solutions with $\omega_B = 0.999713$ and $\omega_B = 0.278990$ (which we will call the "linear" and "nonlinear" breathers, respectively).

Rather than viewing the phase space in the $(q,\ p)$ variables, it is more useful to examine the $(u,\ v)$ space; Figure 2 shows the $(u_1,\ v_1)$ plane, which is a two dimensional projection of the 512 dimensional phase space. Figure 2a shows the phase space for $t \leq 5000$ (50,000 iterations of (9)), for which both solutions are relatively stable. For $t > 5000$ the "nonlinear" breather becomes unstable, as seen in Figure 2b. Looking at the magnitude of these phase space variables, $\rho_1 = \sqrt{(\omega_1^2 + \Gamma^2)u_1^2 + v_1^2}$, gives a sense of the time development of the system. Figure 3 shows the time evolution of mode 1 (the lowest frequency linear mode) over the period of time shown in Figure 2. The lower curve is the "linear" breather, which is stable over long times ($\sim$ 3000 breather periods), while the upper curve (the "nonlinear" breather) is stable over much shorter time periods ($\sim$ 200 breather periods). In both cases the total energy of the system is approximately constant, as seen in Figure 4, so the decay of the "nonlinear" breather in Figure 3 is the result of energy being transferred between modes, not of energy being added to the system. (Nonconstancy of the total energy results from discretizing in time). Snapshots of the time development of the entire spectrum are shown in Figure 5 for the "linear" breather and in Figure 6 for the "nonlinear" breather. In both cases the system has reached an apparent steady state by $t = 20000$. The final energy distribution is very different for the two cases, however: in the nearly linear case, the energy remains in a small number of modes, while in the nonlinear (and higher energy) case, the energy is exchanged between many modes.

3. Parametric Instability

In the previous examples the mapping period was chosen so that the mapping dynamics approximated the behavior of the differential equations (5). In general, however, the discretization in time introduces the possibility of a parametric instability in the system. If the mapping period for the previous example is doubled to $T = 0.2$, then the solutions become unstable as seen in Figure 7. Not only is the solution now unstable on a relatively short time scale, but energy is pumped into the system through the instability. To understand the dynamics in this regime, we linearize H_1 in (6) for small u:

$$\begin{aligned} H_1 &= \Gamma^2 \left(\sum_{i=1}^{N} \left[1 - \cos\left(\sum_{r=1}^{N} u_r e_{ir} \right) \right] \right) \sum_{m=-\infty}^{\infty} \delta(t/T - m) \\ &= \Gamma^2 \left(\sum_{i,r,s=1}^{N} \frac{1}{2} u_r e_{ir} u_s e_{is} \right) \sum_{m=-\infty}^{\infty} \delta(t/T - m) \\ &= \Gamma^2 \sum_{r=1}^{N} \frac{u_r^2}{2} \sum_{m=-\infty}^{\infty} \delta(t/T - m). \end{aligned}$$

The delta functions can be rewritten as

$$\sum_{m=-\infty}^{\infty} \delta(t/T - m) = \sum_{m=-\infty}^{\infty} \cos\frac{2\pi m t}{T}$$

so that the linearized Hamiltonian is

$$H = H_0 + H_1 = \sum_{r=1}^{N} \left(\frac{1}{2} v_r^2 + \frac{\omega_r}{2} u_r^2 \right) + \frac{\Gamma^2}{2} \sum_{r=1}^{N} u_r^2 \sum_{m=-\infty}^{\infty} \cos\frac{2\pi m t}{T}.$$

Transforming to action-angle variables, $u_r = \sqrt{2J_r/\omega_r}\sin\theta_r$, and $v_r = \sqrt{2\omega_r J_r}\cos\theta_r$, we obtain

$$H = \sum_{r=1}^{N} \left[\omega_r J_r + \frac{\Gamma^2 J_r}{\omega_r} \sin^2\theta_r \sum_{m=-\infty}^{\infty} \cos\frac{2\pi m t}{T} \right]. \tag{12}$$

Thus, there can be a resonance in the last term between one (or more) of the linear modes, of frequency $\dot{\theta}_r = \omega_r$ and the driving frequency $\Omega = 2\pi/T$. The resonance will occur whenever $\omega_r T = m\pi$, or $2\omega_r/\Omega = m$. This is the resonance found in the Mathieu equation [13]. Note that since $\omega_{\max} = \omega_{N/2} = 2N/L$, there exists a maximum driving frequency for resonance, $\Omega_{\max} = 4N/L$, or a minimum resonant period $T_{\min} = \pi L/2N$. That is, there are two regimes: if the pulsing period is larger than $T_{\min}$, then it is possible that one (or more) of the linear modes is resonant with the pulsing period, and if $T < T_{\min}$, there is no linear resonance. For the above example, $T_{\min} = 0.1963$.

In the case of resonance, the fixed point at $q = 0$ (when all the pendula are pointing straight down) is unstable, and the resonant mode will grow exponentially. This growth rate can be calculated from the linearized system. In the linear regime, the dynamics of each mode is given by the mapping

$$\begin{pmatrix} u_s' \\ v_s' \end{pmatrix} = \begin{pmatrix} \cos\omega_s T - \Gamma^2 T \sin\omega_s T/\omega_s & \sin\omega_s T/\omega_s \\ -\omega_s \sin\omega_s T - \Gamma^2 T \cos\omega_s T & \cos\omega_s T \end{pmatrix} \begin{pmatrix} u_s \\ v_s \end{pmatrix} = \mathsf{M} \begin{pmatrix} u_s \\ v_s \end{pmatrix}. \qquad (13)$$

The mode will be unstable when $|\mathrm{TrM}| > 2$, with a growth rate given by the eigenvalues $\lambda_\pm = \mathrm{TrM}/2 \pm \sqrt{(\mathrm{TrM}/2)^2 - 1}$. For the $m = 1$ resonance near $\omega_s T \simeq \pi$, the instability condition becomes

$$\pi > \omega_s T > \frac{\pi\omega_s^2}{\Gamma^2 + \omega_s^2}. \qquad (14)$$

Since the linear frequencies are doubly degenerate ($\omega_s = \omega_{N-s}$), two modes will be unstable when (14) is satisfied. For the case above, with $T = 0.2$, modes 112 and 144 ($= 256 - 112$), with frequency $\omega_{112} = \omega_{144} = 16\sin(112\pi/256) = 15.69$ are unstable, and grow exponentially for $0 < t < 1000$, as shown in Figure 8. In this case, $\mathrm{TrM} = -2.0000298$, yielding to eigenvalues of $\lambda_+ = -0.99456$ and $\lambda_- = -1.00547$, the latter of which corresponds to the exponential growth seen in Figure 8. Snapshots of the time evolution of the entire spectrum are shown in Figure 9.

This instability results from the interaction of the spatial and temporal discreteness. As the spatial lattice is made finer, the number of modes increases, and the maximum linear frequency, $\omega_{N/2} = 2N/L$, approaches infinity. To examine the behavior of the instability as $N \to \infty$, we calculate the maximum growth rate as $\omega_s \to \infty$. That is, we calculate

$$\alpha = \lim_{\omega_s \to \infty} \frac{1}{T} \ln |\lambda_-|,$$

subject to the constraint that TrM is maximized. We find that $\alpha \simeq \Gamma^2/2\omega_s \to 0$ as ω_s approaches infinity; that is, that the maximum growth rate of an unstable mode is inversely proportional to the frequency of that mode. Thus, the instability disappears as $N \to \infty$ and $T \to 0$ independent of the order in which the limits are taken.

Because the preceding analysis is linear, it neglects both the saturation of the instability, seen in Figure 8 for $t > 1000$, and the energy transfer between the linear modes, as seen in Figure 9. To look at these in greater detail, we examine the case where two modes with the same harmonic frequency (ω_r and ω_{N-r}) are much larger than any of the others. That is, we write

$$\sum_{r=1}^{N} u_r e_{ir} = u_b e_{ib} + u_{N-b} e_{i,N-b} + \sum_{r'=1}^{N} u_{r'} e_{ir'},$$

where the prime denotes summation over all modes except modes b and $N-b$. This will be the case when there is an instability in the system which dominates the dynamics. We assume that $u_{r'} \ll u_b$, and expand H_1 in (6):

$$H_1 = \Gamma^2 \sum_{m=-\infty}^{\infty} \delta(t/T - m) \sum_{i=1}^{N} \left[1 - \cos\left(u_b e_{ib} + u_{N-b} e_{i,N-b} + \sum_{r'=1}^{N} u_{r'} e_{ir'} \right) \right].$$

Note that

$$e_{ib} = \frac{1}{\sqrt{N}}\left(\cos\frac{2\pi ib}{N} - \sin\frac{2\pi ib}{N}\right),$$
$$e_{i,N-b} = \frac{1}{\sqrt{N}}\left(\cos\frac{2\pi ib}{N} + \sin\frac{2\pi ib}{N}\right),$$

so that we may write H_1 as

$$\begin{aligned} H_1 &= \Gamma^2 \sum_{m=-\infty}^{\infty} \delta(t/T - m) \\ &\quad \times \sum_{i=1}^{N}\left[1 - \cos\left(\frac{u_b + u_{N-b}}{\sqrt{N}}\cos\frac{2\pi ib}{N} - \frac{u_b - u_{N-b}}{\sqrt{N}}\sin\frac{2\pi ib}{N} + \sum_{r'=1}^{N} u_{r'}e_{ir'}\right)\right] \\ &= \Gamma^2 \sum_{m=-\infty}^{\infty} \delta(t/T - m) \\ &\quad \times \sum_{i=1}^{N}\left[1 - \cos\left(\frac{u_b + u_{N-b}}{\sqrt{N}}\cos\frac{2\pi ib}{N} - \frac{u_b - u_{N-b}}{\sqrt{N}}\sin\frac{2\pi ib}{N}\right)\cos\left(\sum_{r'=1}^{N} u_{r'}e_{ir'}\right)\right. \\ &\qquad \left. + \sin\left(\frac{u_b + u_{N-b}}{\sqrt{N}}\cos\frac{2\pi ib}{N} - \frac{u_b - u_{N-b}}{\sqrt{N}}\sin\frac{2\pi ib}{N}\right)\sin\left(\sum_{r'=1}^{N} u_{r'}e_{ir'}\right)\right]. \qquad (15) \end{aligned}$$

The dominant terms (u_b and u_{N-b}), have been separated from the remaining terms. To examine the dynamics of these modes, we expand (15) in terms of Bessel functions, keeping only the zeroth order terms in $u_{r'}$:

$$\begin{aligned} H &= \frac{v_b^2 + v_{N-b}^2}{2} + \frac{\omega_b^2}{2}(u_b^2 + u_{N-b}^2) \\ &\quad + N\Gamma^2 \sum_{m=-\infty}^{\infty} \delta(t/T - m)\left[1 - J_0\left(\frac{u_b + u_{N-b}}{\sqrt{N}}\right) J_0\left(\frac{u_b - u_{N-b}}{\sqrt{N}}\right)\right. \\ &\qquad \left. + 2J_2\left(\frac{u_b + u_{N-b}}{\sqrt{N}}\right) J_2\left(\frac{u_b - u_{N-b}}{\sqrt{N}}\right)\right]. \end{aligned}$$

Again using the boundary conditions (8), we obtain a four dimensional map in terms of the sum and difference variables

$$x_\pm = \frac{u_b \pm u_{N-b}}{\sqrt{2}}, \qquad y_\pm = \frac{v_b \pm v_{N-b}}{\sqrt{2}}:$$

$$\begin{pmatrix} x'_\pm \\ y'_\pm \end{pmatrix} = \begin{pmatrix} \cos\omega_b T & \sin\omega_b T/\omega_b \\ -\omega_b \sin\omega_b T & \cos\omega_b T \end{pmatrix} \begin{pmatrix} x_\pm \\ y_\pm \end{pmatrix}$$

$$- \sqrt{2N}\Gamma^2 T \left(J_1^\pm \left(J_0^\mp + J_2^\mp\right) - J_3^\pm J_2^\mp\right) \begin{pmatrix} \sin\omega_b T/\omega_b \\ \cos\omega_b T \end{pmatrix}. \tag{16}$$

Here $J_n^\pm \equiv J_n(\sqrt{2/N}x_\pm)$. In the linear regime near the fixed point, these maps uncouple into two sets of two dimensional maps of the form (13).

The system (16) reproduces the dynamics of the full system very well when one or two modes dominate the dynamics. Additionally, saturation of the instability is described by this map. By looking at the trace of (16), we can modify the instability condition (14):

$$\pi > \omega_s T > \frac{\pi\omega_s^2}{(1-(u_b^2+u_{N-b}^2)/4N)\Gamma^2+\omega_s^2}. \tag{17}$$

If the initial configuration is sufficiently energetic (that is, if u_b or u_{N-b} is large enough), the linear parametric resonance will be suppressed by the nonlinearity, and the fixed point at $(0,0)$ will again be elliptic. This has been observed in numerical results from both the entire system (9) and the reduced system (16).

By choosing an initial condition with all the energy in a single mode, we can compare the behavior of (16) to (9) by looking at the two dimensional phase space of that mode. For example, for the above parameters, with the pulsing period increased to $T = 0.25$, mode 73 will be unstable. We start with all the energy in that mode, and let the entire system (9) evolve. Figure 10 shows the (u_{73}, v_{73}) space given such an set of initial conditions. This should be compared with Figure 11a, which shows the evolution of (16) for the same set of initial conditions. These show quite clearly the hyperbolic fixed point with reflection at the origin, $(u,v) = (0,0)$, that exists in the unstable regime (when $\omega_b T \lesssim \pi$). As T is varied to move the system out of the resonant region (equation (14)), the system undergoes a bifurcation and the origin becomes an elliptic fixed point, as shown in Figure 11b.

For initial conditions near the hyperbolic point, the situation is slightly more complicated. Since the subsequent trajectory is sensitively dependent on how close the orbit approaches the fixed point, the other modes act to perturb the trajectory, as seen in Figure 12a. This can be reproduced in (16) by adding a small amount of noise to the map, as seen in Figure 12b. Hence, (16) is seen to well describe the full dynamics of (9) when two modes dominate the dynamics, including the effects of parametric instability and nonlinear saturation.

4. Conclusion

In this paper we have primarily been concerned with the parametric instabilities that arise when the Sine-Gordon equation is discretized in space and time. This resonance occurs when the frequency of time discretization is sufficiently small. We have determined the instability condition and calculated the growth rates of the unstable modes. We have also shown that the maximum growth rate decreases inversely with the frequency, so that the instability disappears when the discreteness is made infinitely fine. Additionally, by examining the effects of two finite amplitude modes, we have described the nonlinear saturation of the instability.

Still unanswered is the larger question of how the discretized system approaches the behavior of the continuous system for finer and finer discretizations in the regime where the parametric instability is absent. Of particular interest is how the soliton solutions of the continuous system behave for different amounts of discretization. Such solutions are clearly unstable if the discretization of the system is too coarse, and the energy is spread among the oscillators. How (and whether) these solutions become stable as $N \to \infty$ and $T \to 0$ is not understood, however. Figures 5 and 6 indicate that there may be some critical parameter (such as the energy density, as proposed in [8] for the Fermi-Pasta-Ulam problem) that determines, for a particular discretization, when a soliton solution will be stable and when there will be equipartition among the oscillators. These questions are currently under investigation.

Acknowledgments

The support for this work was provided by National Science Foundation Grant ECS-8517364 and Office of Naval Research Contract N00014-84-K-0367.

Figure Captions

Figure 1. The initial breather configuration. —— The "nonlinear" breather with $\omega_B = 0.278990$; - - - the "linear" breather with $\omega_B = 0.999713$.

Figure 2. The (u_1, v_1) space: $N = 256$, $L = 32$, $T = 0.1$. The outer curve is the "nonlinear" breather, the inner curve is the "linear" breather. a) $t \leq 5000$. b) $5000 < t < 20000$. Note that the "nonlinear" breather decays at $t \sim 5000$.

Figure 3. The time evolution of $\rho_1 = \sqrt{(\omega_1^2 + \Gamma^2)u_1^2 + v_1^2}$ for the same parameters as Figure 2. The upper curve is the "nonlinear" breather, which decays to a chaotic state at $t \sim 5000$, while the lower curve is the "linear" breather, which is stable.

Figure 4. The total energy in the system. The minor variation is due to the temporal discreteness. The lower curve corresponds to the "linear" breather, the upper to the "nonlinear" breather.

Figure 5. The time evolution of the spectrum of the "linear" breather. Plotted on the vertical axis is $\rho = \sqrt{(\omega^2 + \Gamma^2)u^2 + v^2}$. a) t=0, b) t=5000, c) t=10000, d) t=20000.

Figure 6. The time evolution of the spectrum of the "nonlinear" breather. a) t=0, b) t=5000, c) t=10000, d) t=20000.

Figure 7. The total energy in the system with the "linear" breather as the initial condition as in Figure 4. Here $T = 0.2$, which leads to a parametric instability. Note the difference in both the horizontal and vertical scales as compared to Figure 4.

Figure 8. The time evolution of mode 112 showing its exponential growth when the mapping period is doubled to $T = 0.2$.

Figure 9. The time development of the spectrum of "linear" breather in the unstable regime. a) t=500, b) t=1000, c) t=1500, d) t=2000.

Figure 10. A two dimensional projection of the $2N$ dimensional phase space showing the dominant mode in the unstable regime. $N = 256$, $L = 32$, $T = 0.2$.

Figure 11. A two dimensional projection of the four dimensional phase space of the dominant modes. a) The same parameters as Figure 10, so the instability condition of equation (14) is met, resulting in a hyperbolic fixed point with reflection. b) The mapping period is lowered to $T = 0.1$, so the fixed point is elliptic.

Figure 12. The trajectory near the unstable fixed point. a) A projection of the $2N$ dimensional phase space, showing the effect of the remaining modes on the dominant mode. b) The four dimensional mapping with noise added to simulate the effect of the other trajectories.

References

[1] A. J. Lichtenberg and M. A. Lieberman, *Regular and Stochastic Motion* Springer-Verlag, N. Y. 1983.

[2] E. Fermi, J. R. Pasta and S. Ulam, "Studies of Nonlinear Problems" in *Collected Works of Enrico Fermi* University of Chicago Press, Chicago 1965.

[3] R. L. Bivins, N. Metropolis and J. R. Pasta, J. Comput. Phys. 12 65 (1973).

[4] J. Ford and J. Waters, J. Math. Phys. 4 1293 (1963).

[5] F. M. Izrailev and B. V. Chirikov, Sov. Phys. Dokl. 11 30 (1966).

[6] B. Callegari, M. C. Carotta, C. Ferrario, G. Lo Vecchio and L. Galgani, Nuovo Cimento 54B 463 (1979).

[7] R. Livi, M. Pettini, S. Ruffo, M. Sparpaglione and A. Vulpiani, Phys. Rev. A 28 3544 (1983).

[8] R. Livi, M. Pettini, S. Ruffo, M. Sparpaglione and A. Vulpiani, Phys. Rev. A 31 1039 (1985).

[9] M. D. Kruskal and N. J. Zabusky, J. Math. Phys. 5 231 (1964).

[10] G. Eilenberger, *Solitons* Springer-Verlag, N. Y. 1981.

[11] R. K. Dodd, J. C. Eilbeck, J. D. Gibbon and H. C. Morris, *Solitons and Nonlinear Wave Equations* Academic Press, London 1982.

[12] B. V. Chirikov, Phys. Reports, 52 265 (1979).

[13] V. I. Arnold, *Mathematical Methods of Classical Mechanics* Springer-Verlag, N. Y. 1978.

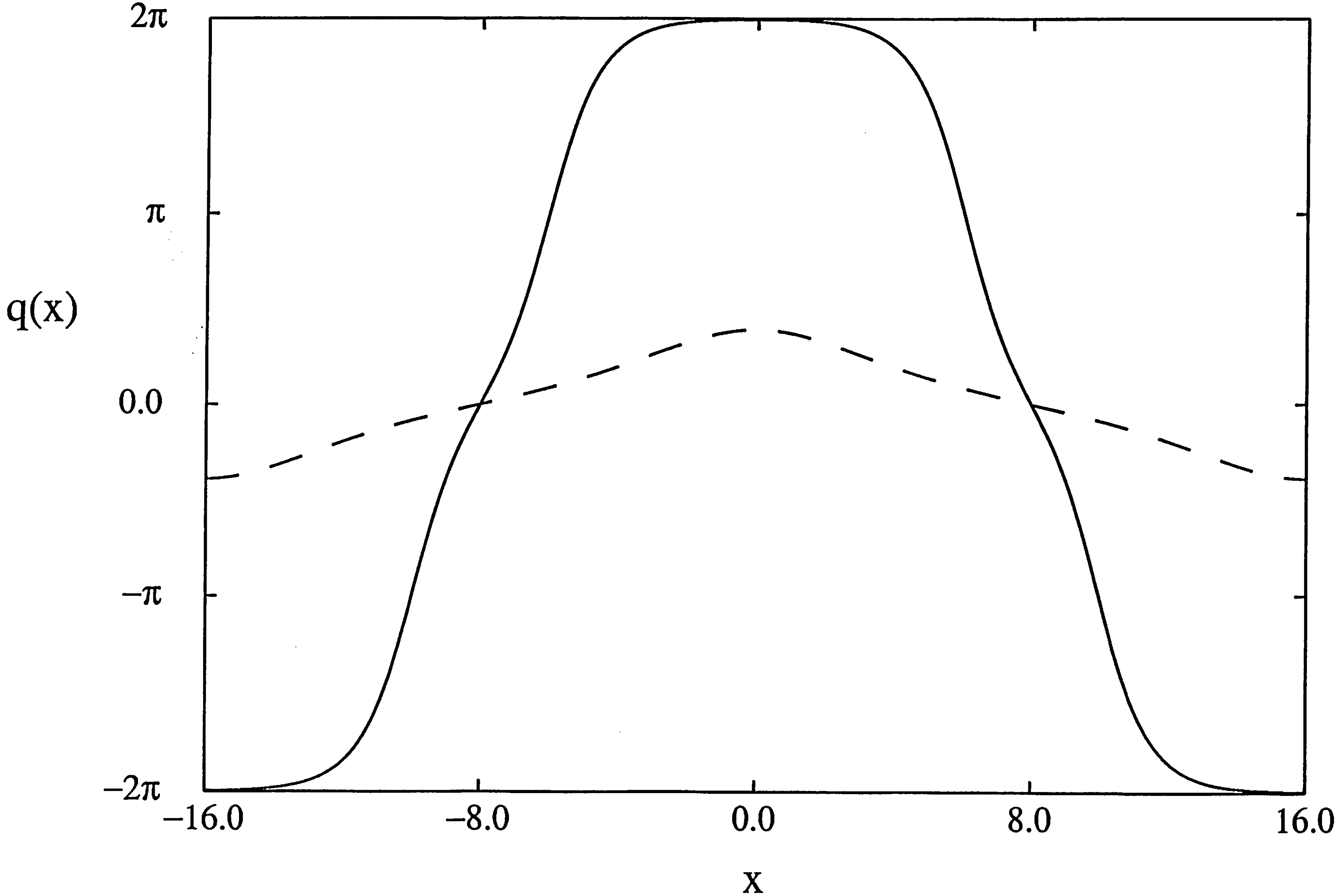
q(x)
2π
π
0.0
−π
−2π
−16.0
−8.0
0.0
8.0
16.0
x

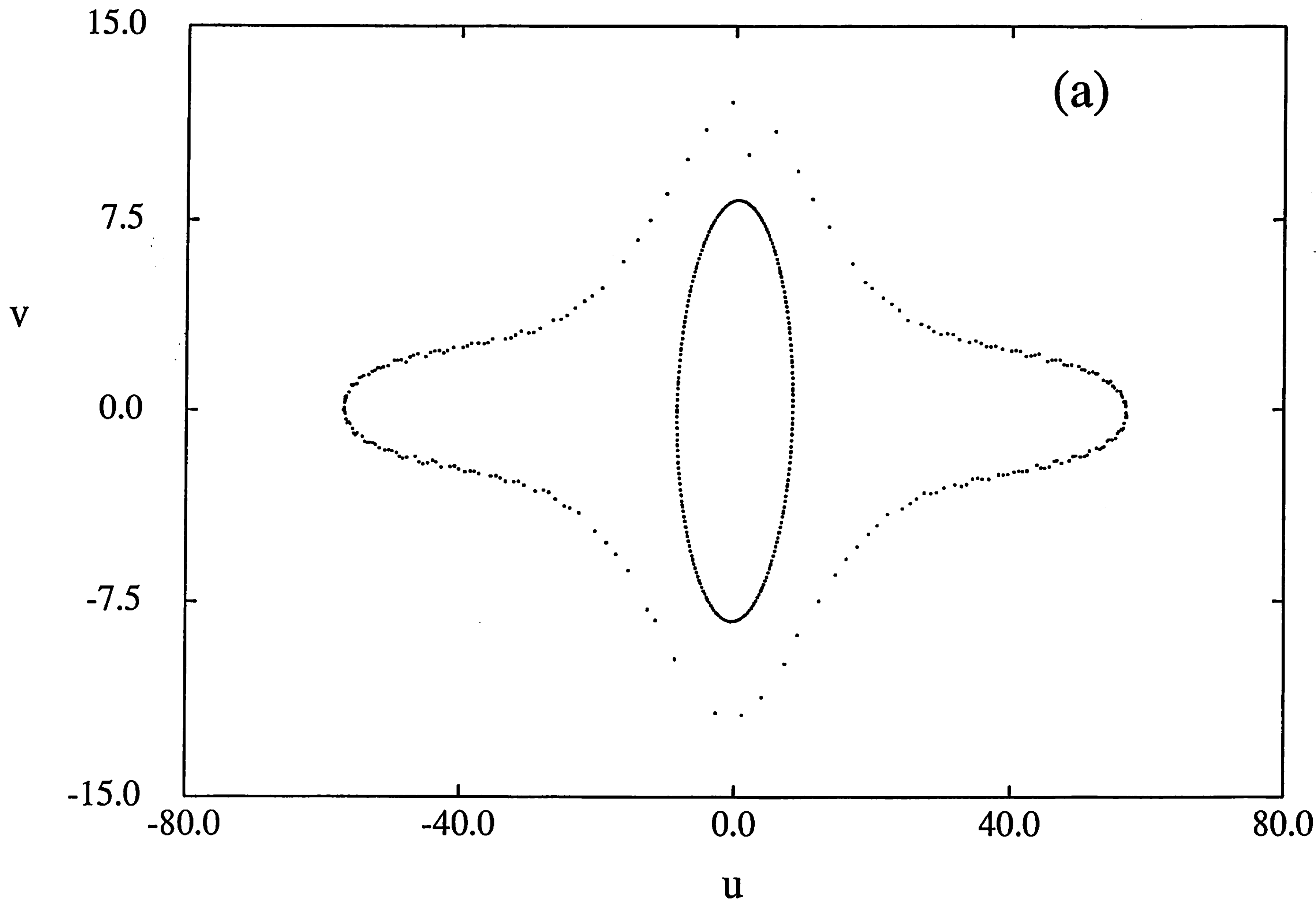
(a)
15.0
7.5
0.0
-7.5
-15.0
v
-80.0
-40.0
0.0
40.0
80.0
u

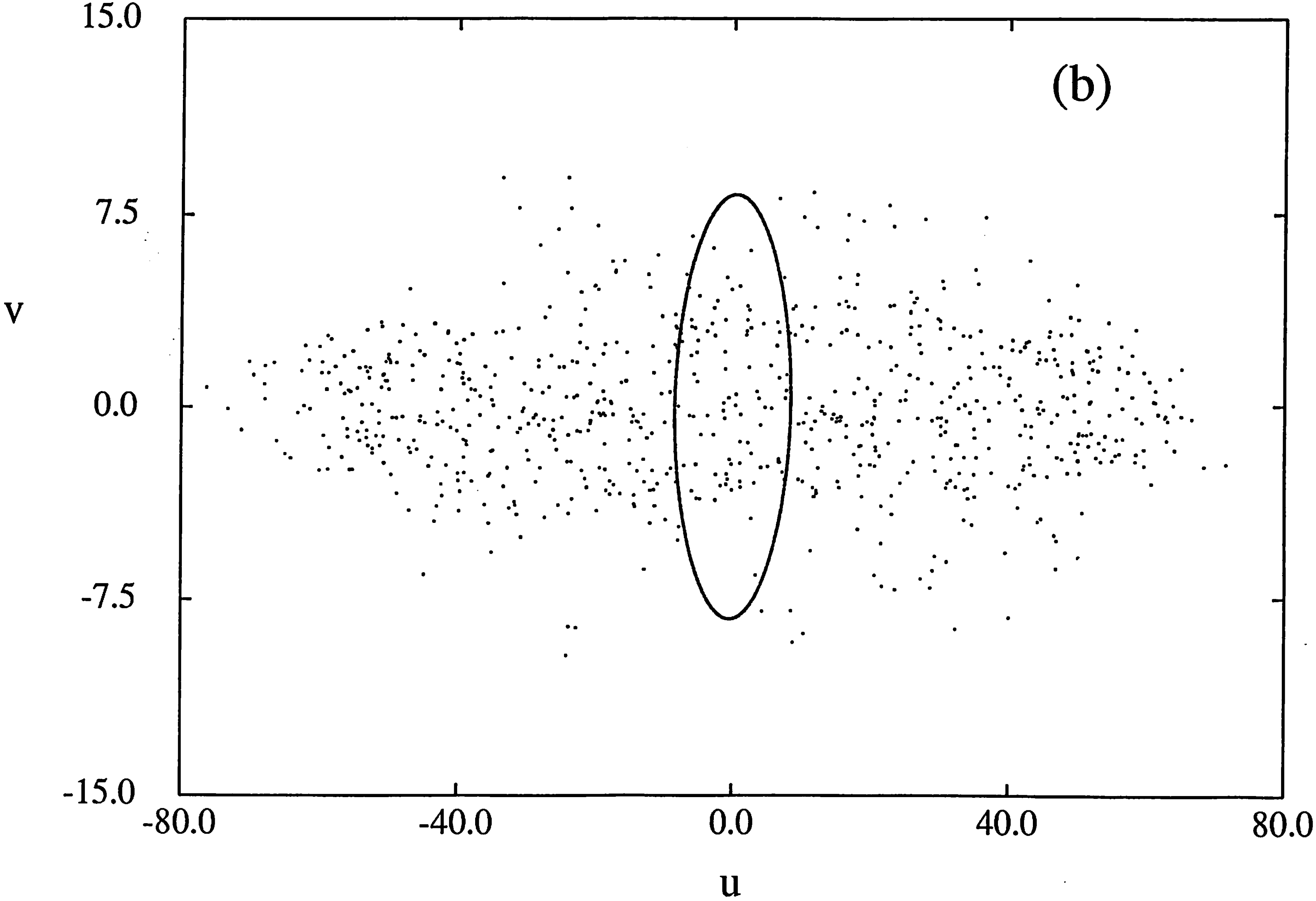
(b)
v
u
15.0
7.5
0.0
-7.5
-15.0
-80.0
-40.0
0.0
40.0
80.0

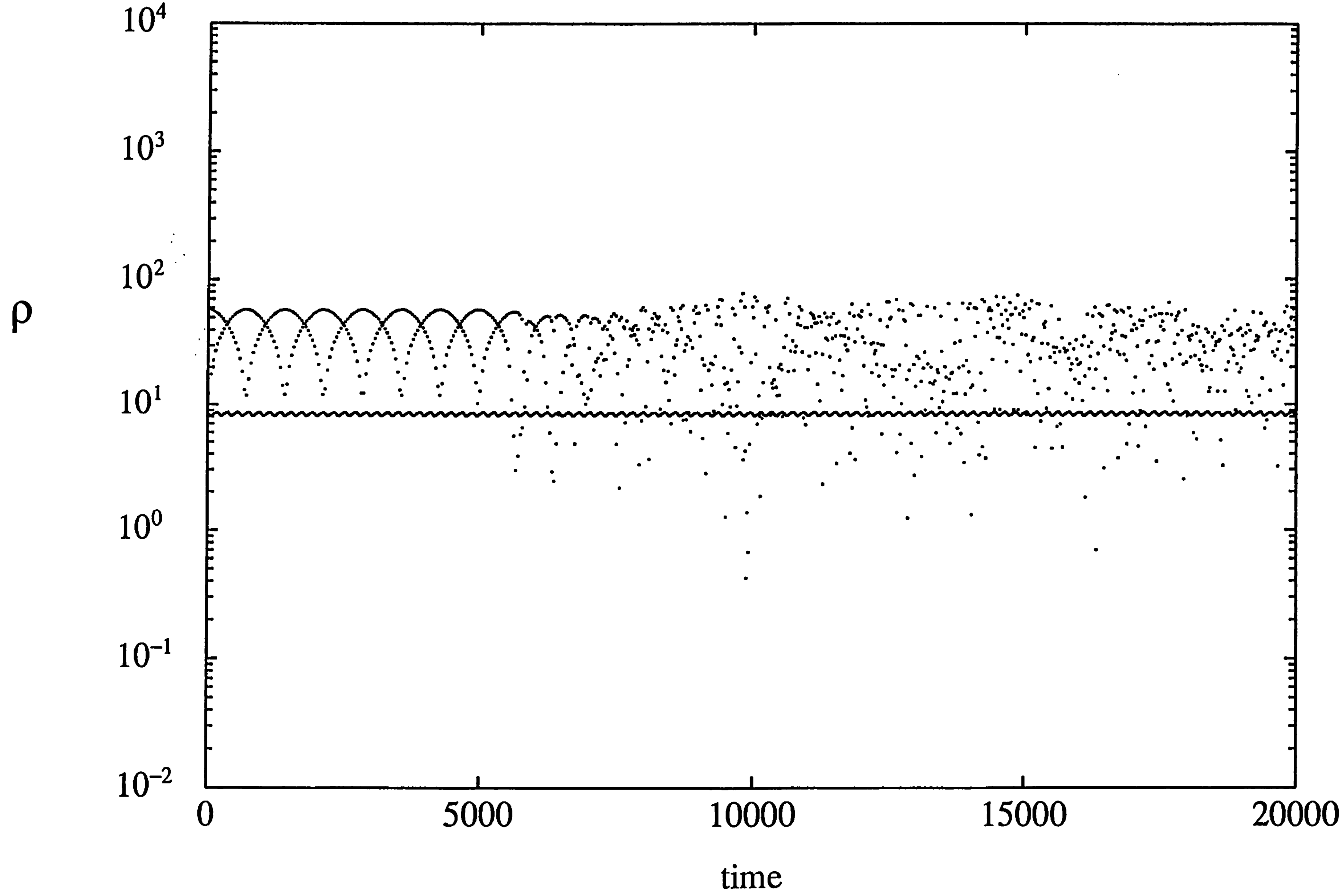

ρ
10^4
10^3
10^2
10^1
10^0
10^{-1}
10^{-2}
0
5000
10000
15000
20000
time

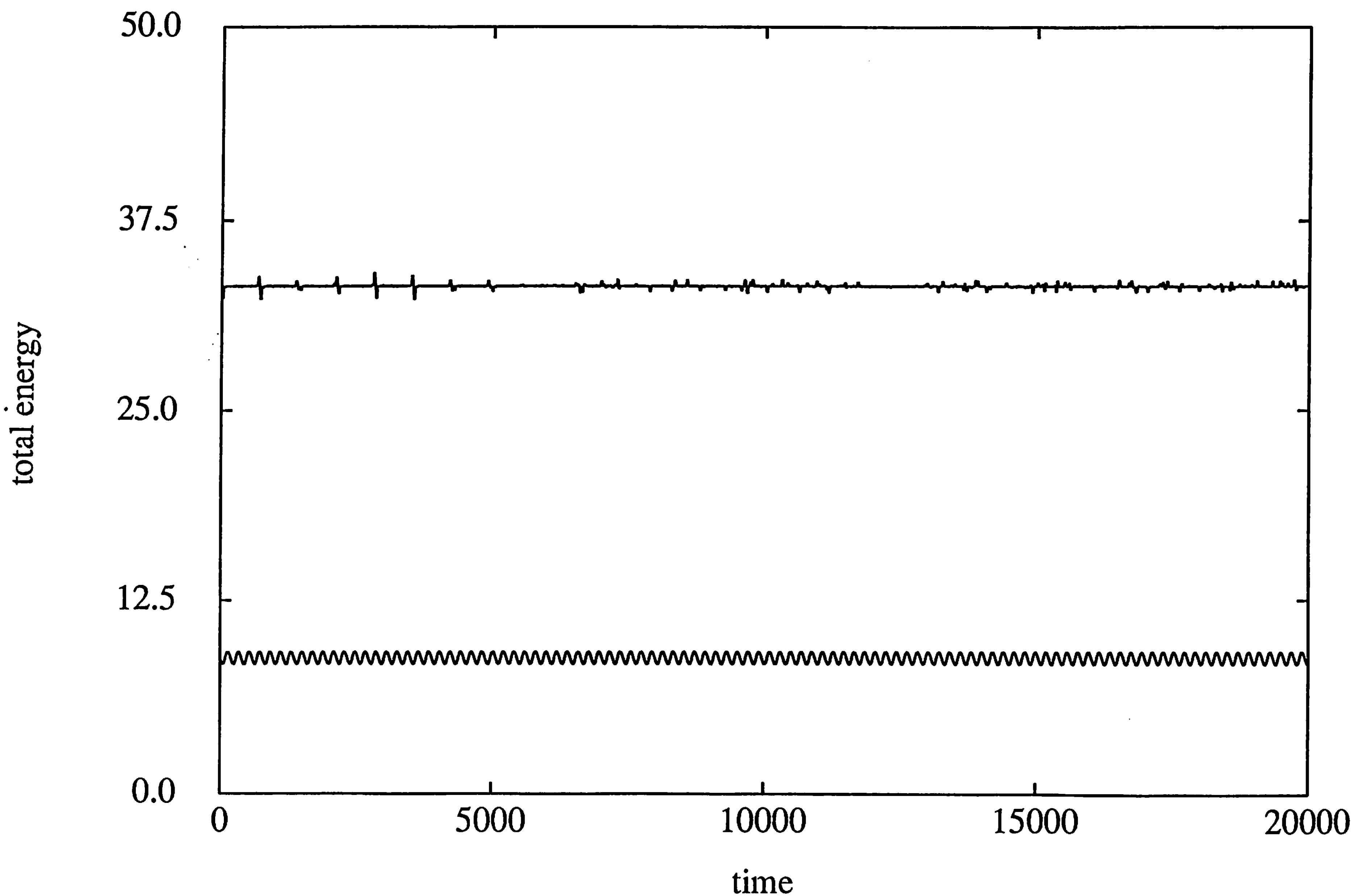

50.0
37.5
25.0
12.5
0.0
total energy
0
5000
10000
15000
20000
time

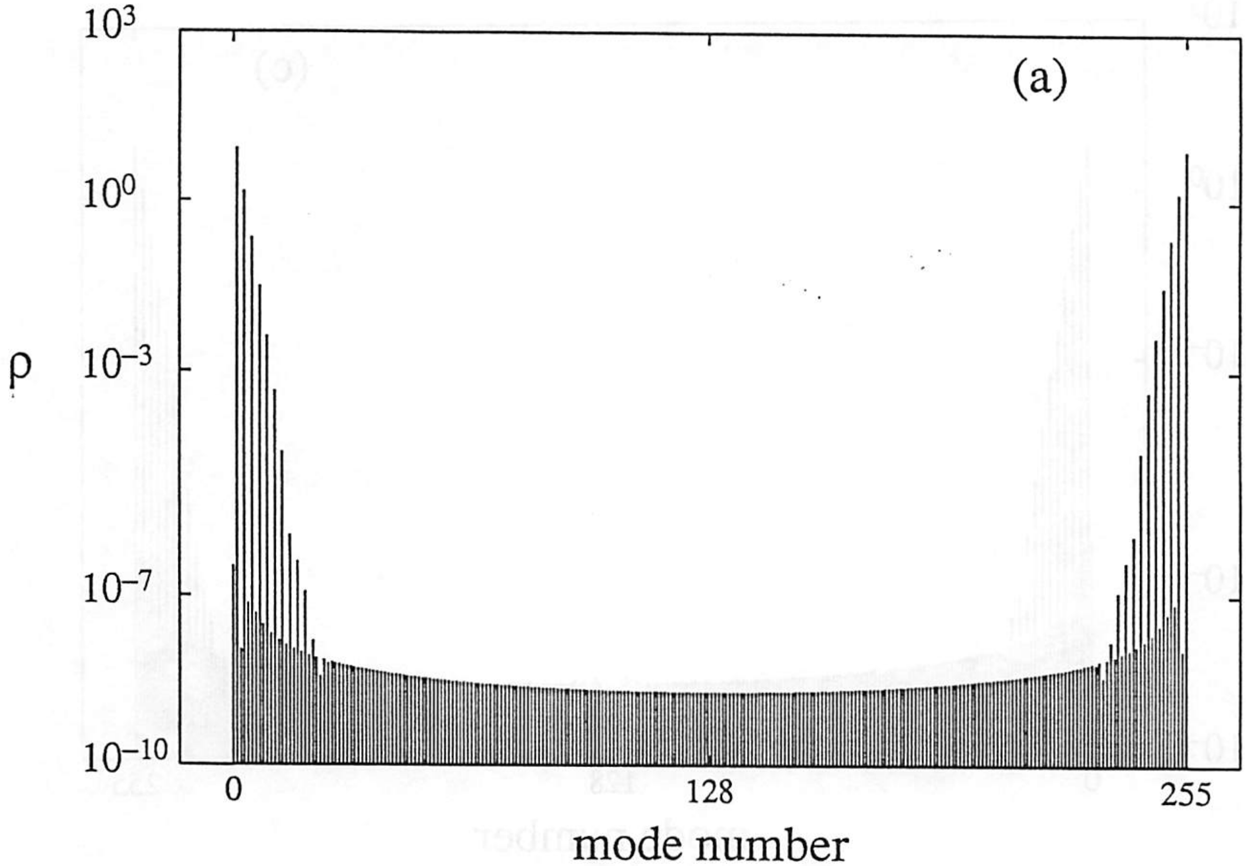
(a)
ρ
10^3
10^0
10^−3
10^−7
10^−10
0
128
255
mode number

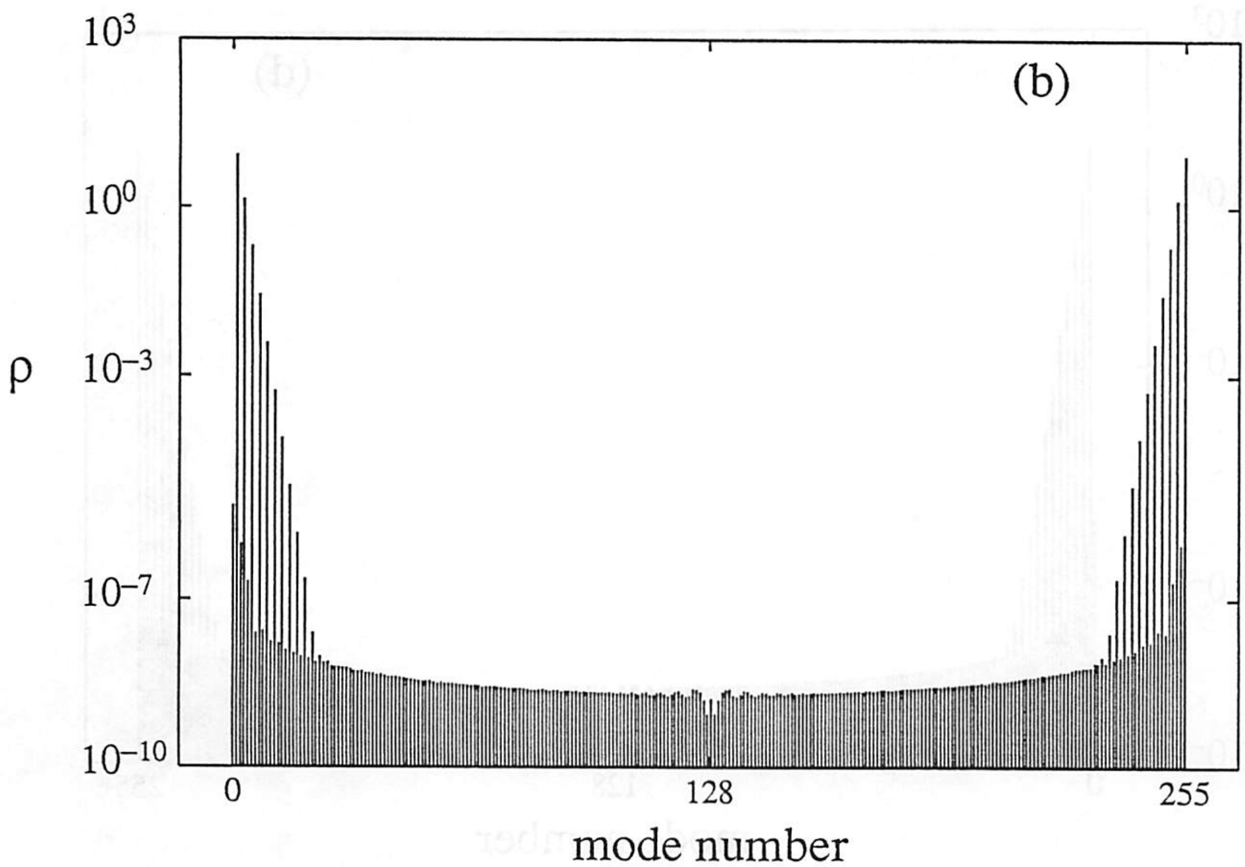
(b)
ρ
10^3
10^0
10^−3
10^−7
10^−10
0
128
255
mode number

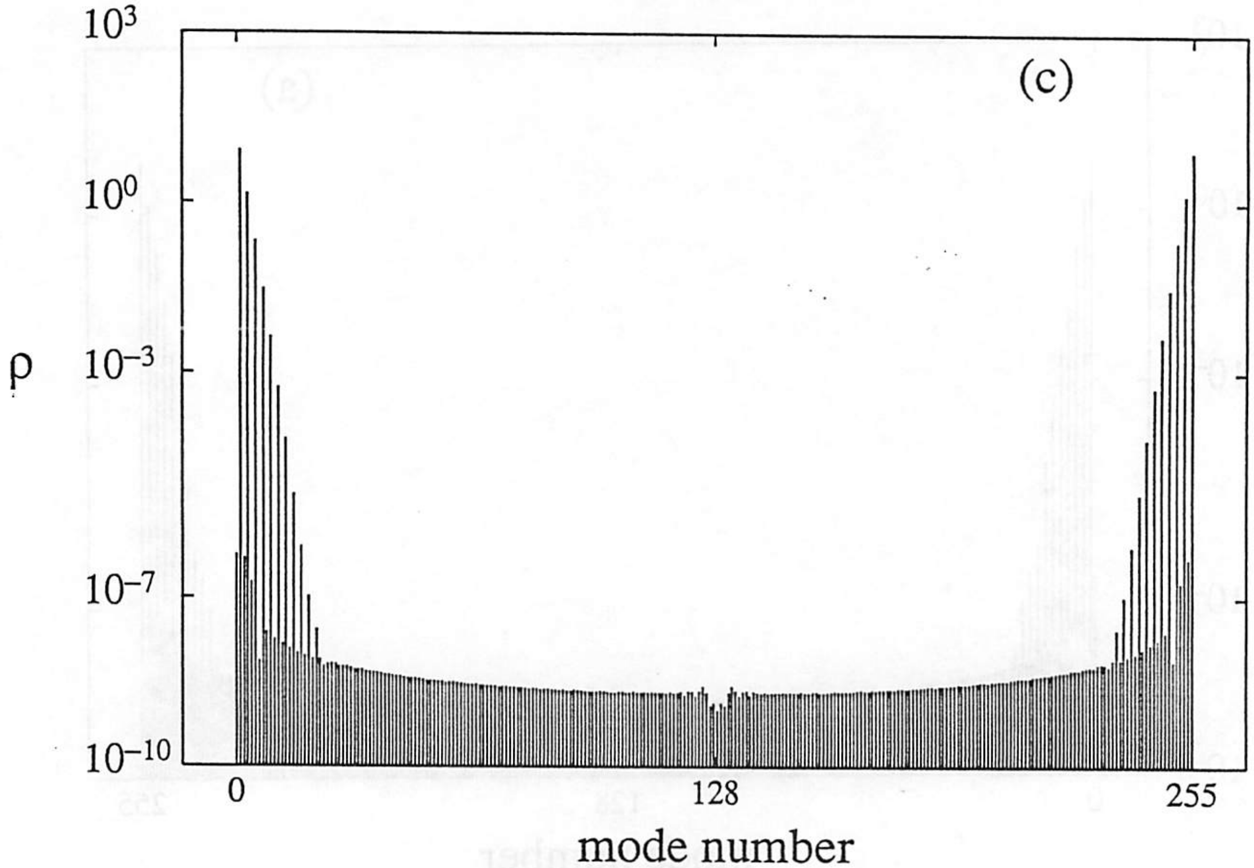

10^3
(c)
10^0
ρ
10^{-3}
10^{-7}
10^{-10}
0
128
255
mode number

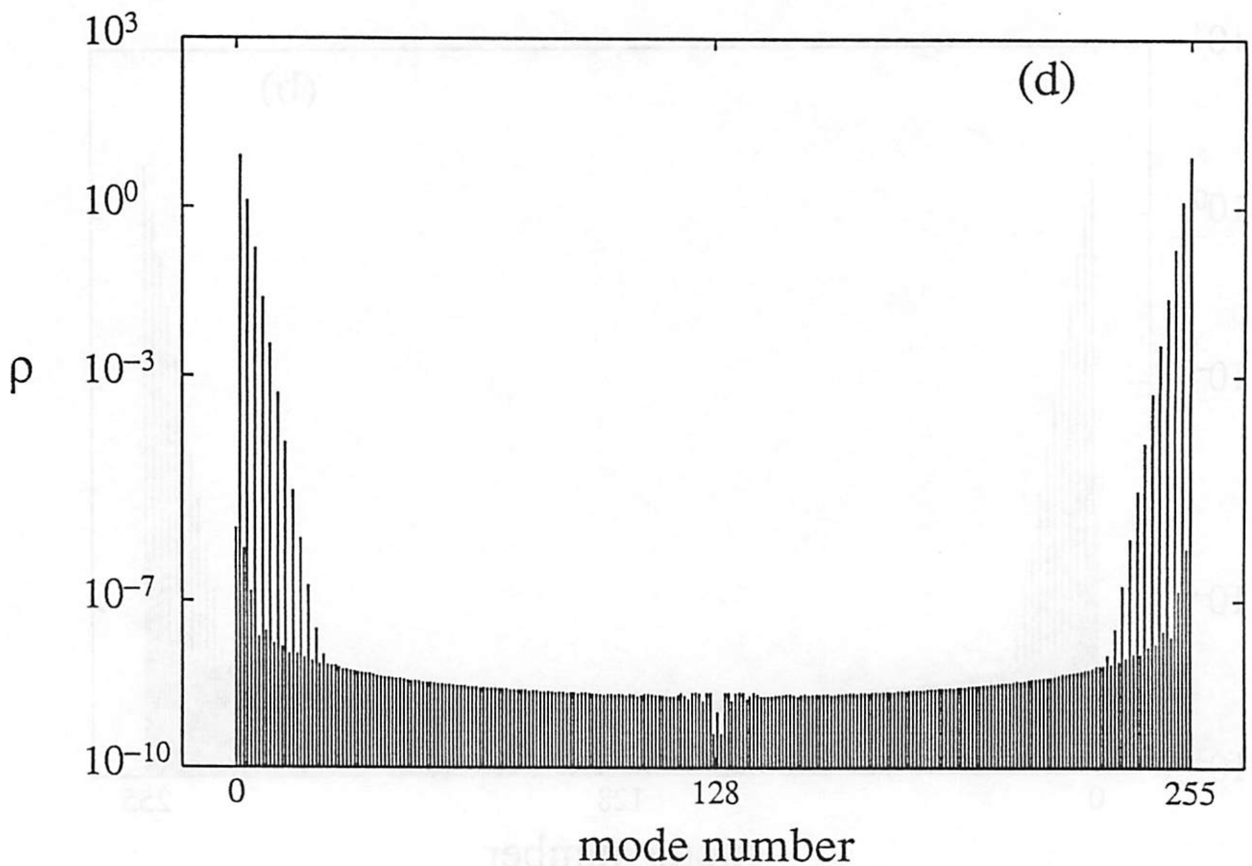

10^3
(d)
10^0
ρ
10^{-3}
10^{-7}
10^{-10}
0
128
255
mode number

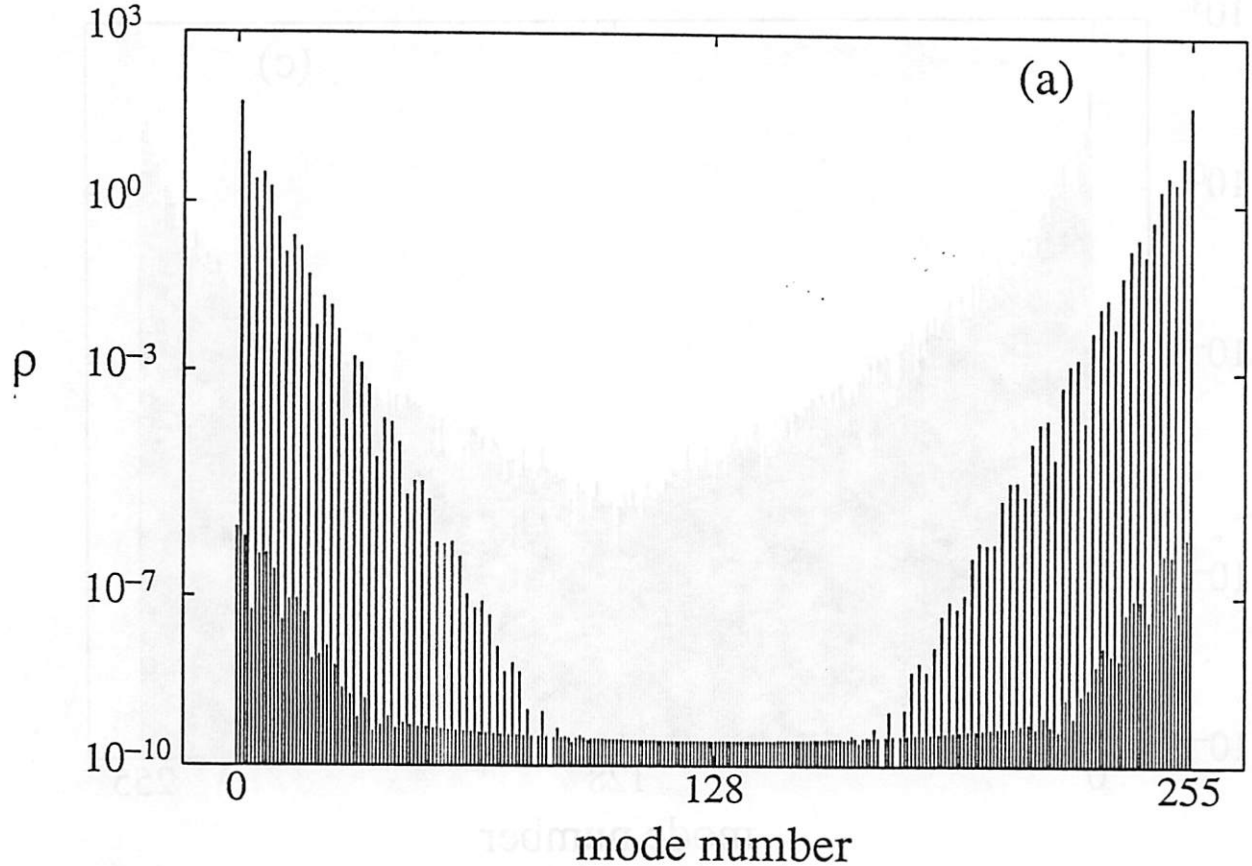

(a)
10^3
10^0
10^-3
10^-7
10^-10
ρ
0
128
255
mode number

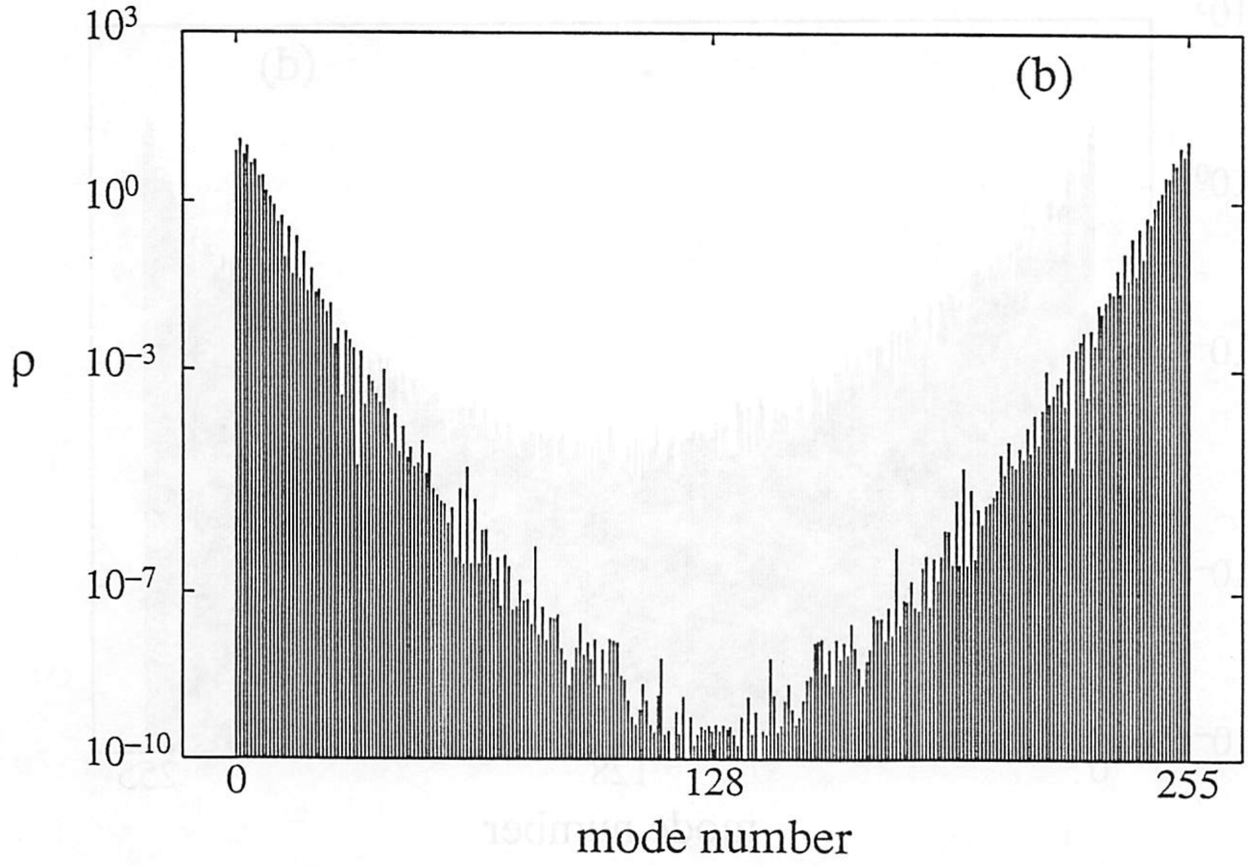

(b)
10^3
10^0
10^-3
10^-7
10^-10
ρ
0
128
255
mode number

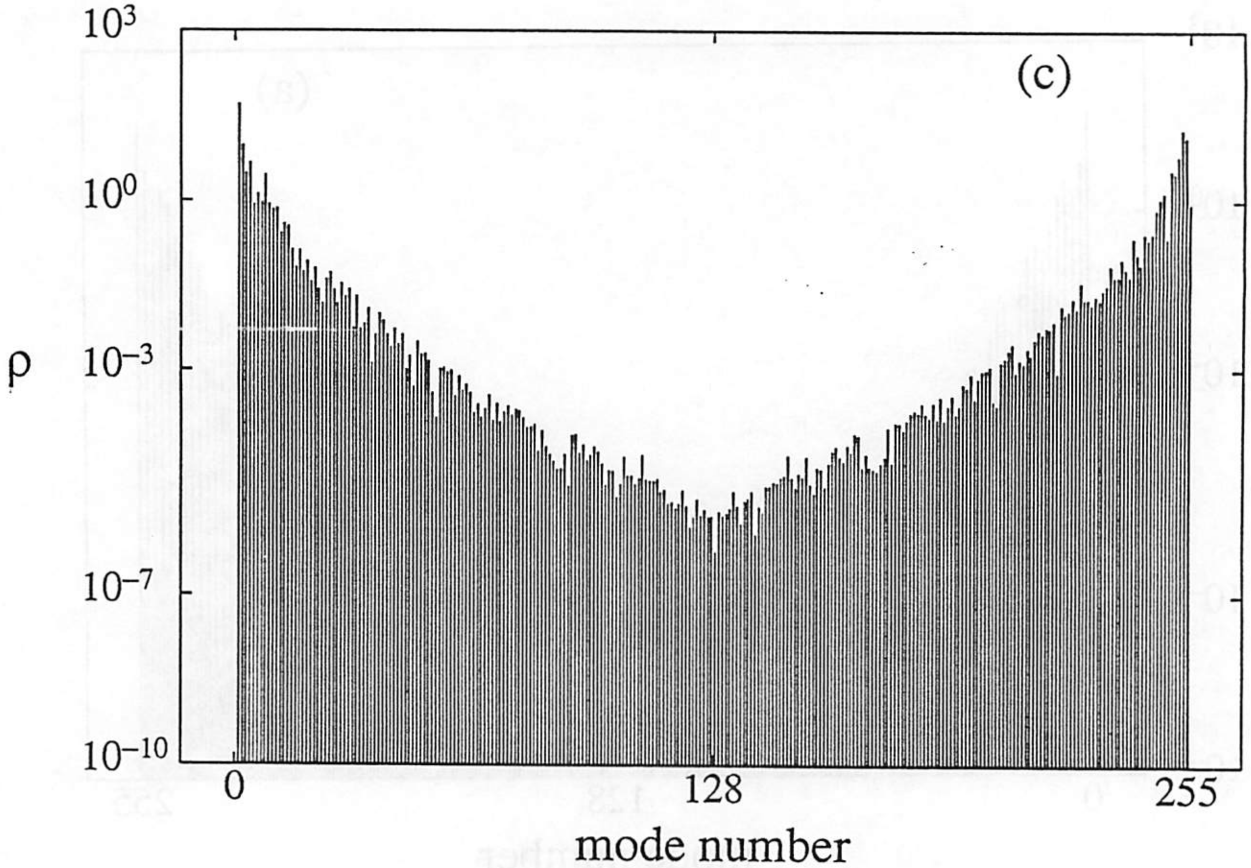
(c)
ρ
10^3
10^0
10^{-3}
10^{-7}
10^{-10}
0
128
255
mode number

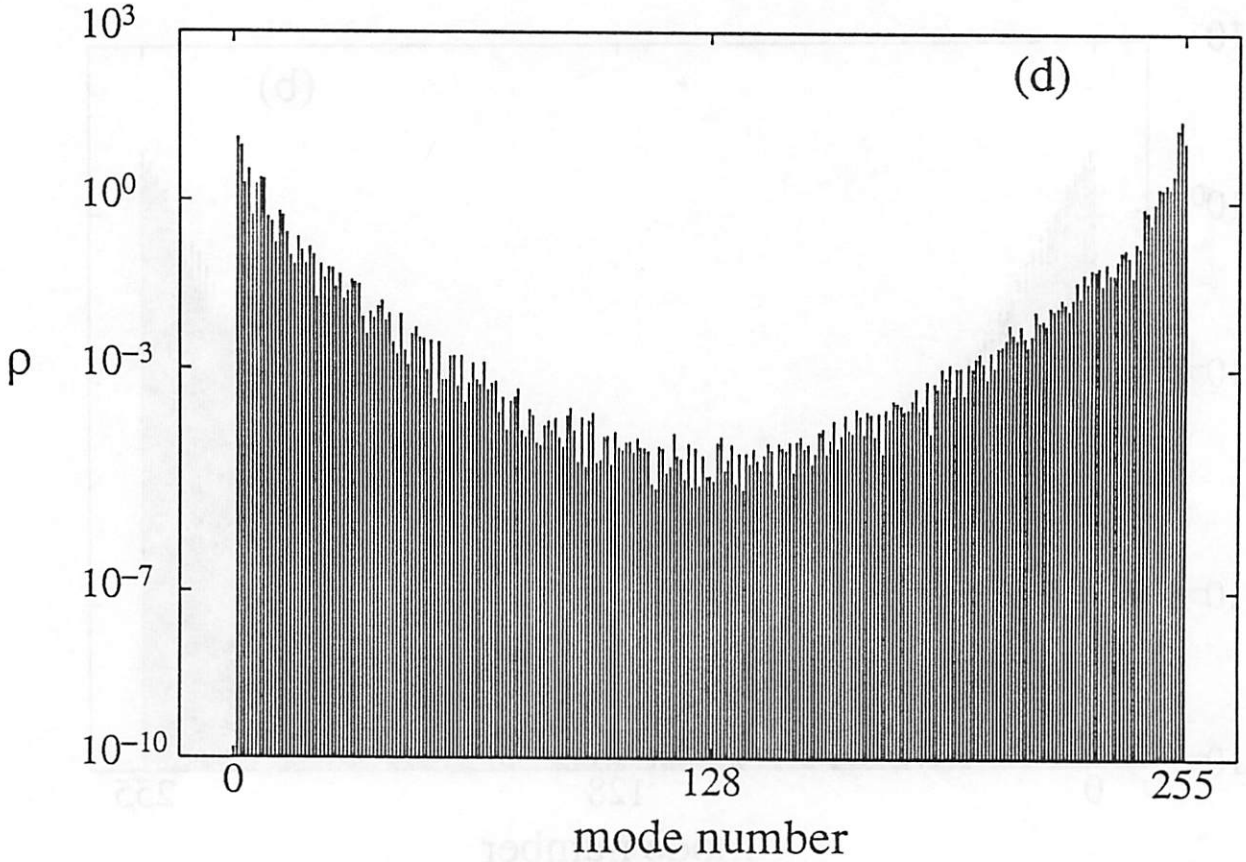
(d)
ρ
10^3
10^0
10^{-3}
10^{-7}
10^{-10}
0
128
255
mode number

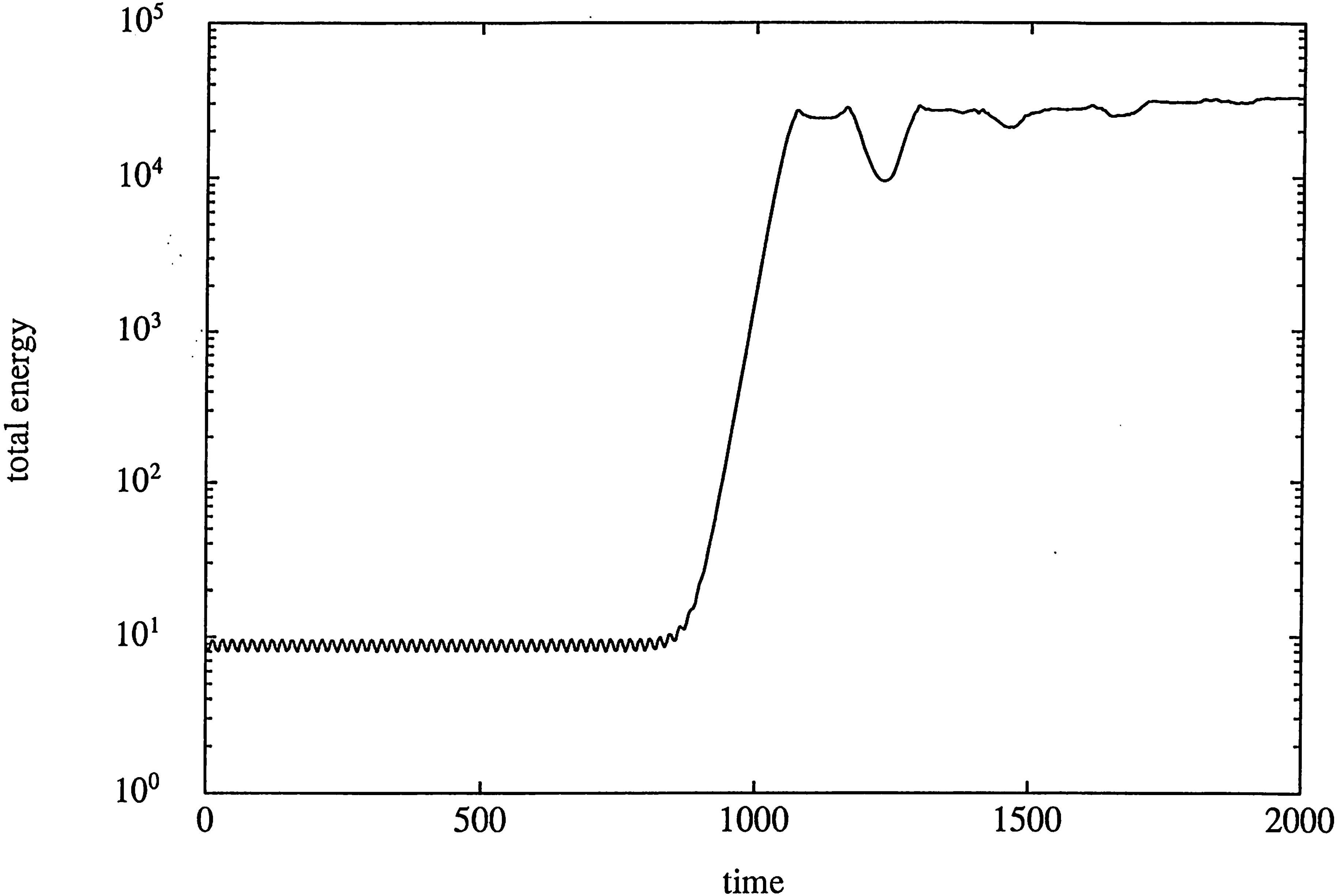

10^5
10^4
10^3
10^2
10^1
10^0
total energy
0
500
1000
1500
2000
time

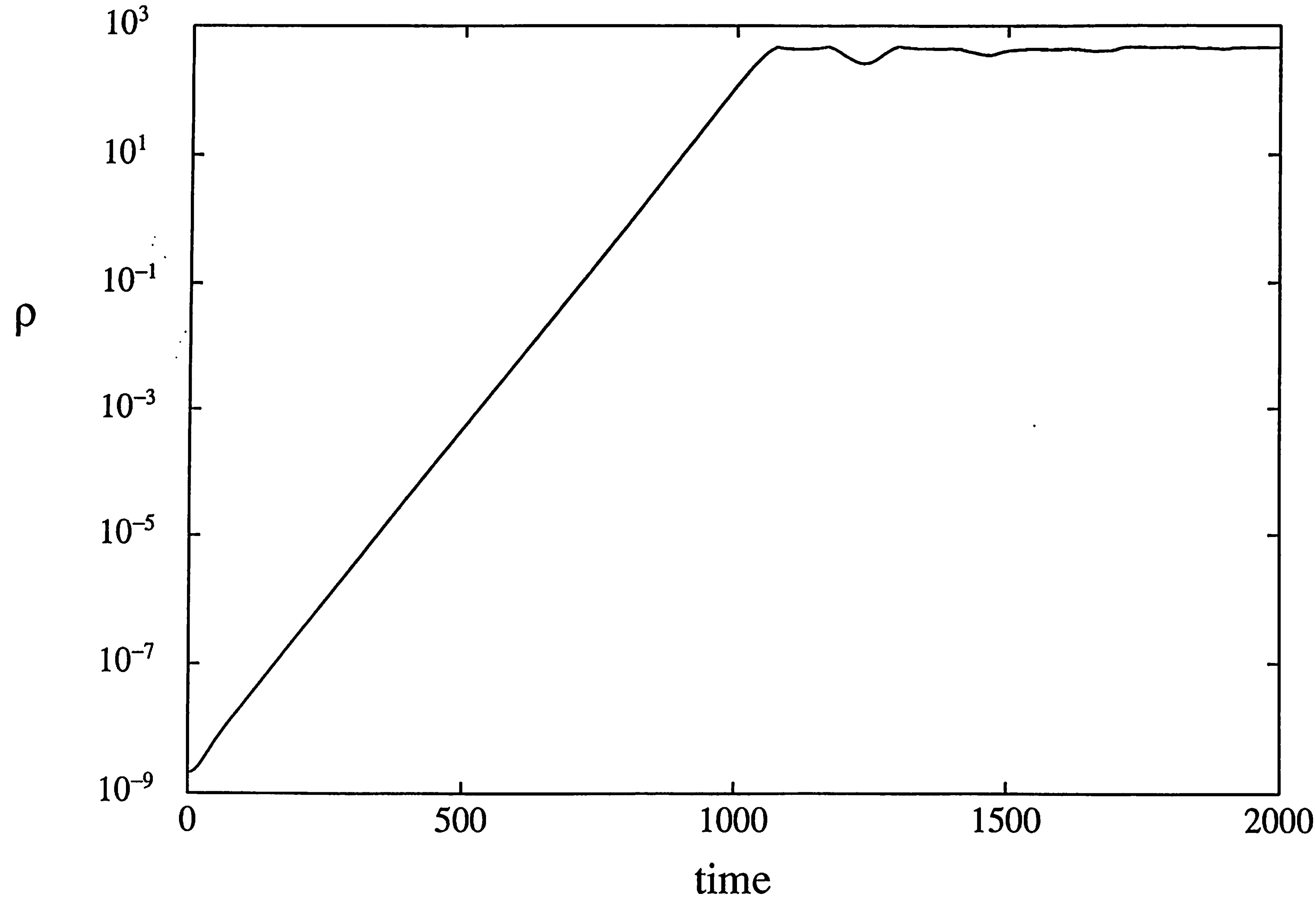

ρ
10^3
10^1
10^-1
10^-3
10^-5
10^-7
10^-9
0
500
1000
1500
2000
time

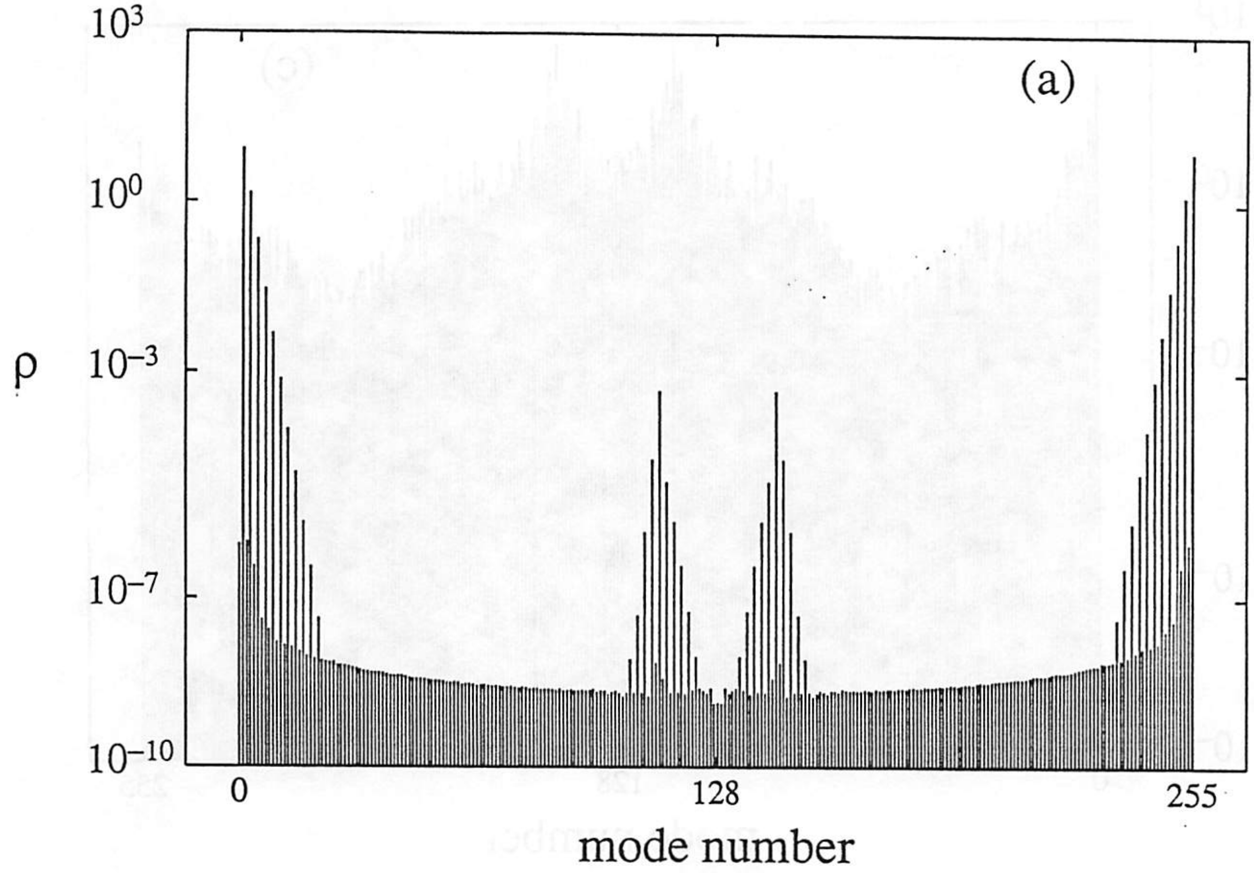

(a)
ρ
10^3
10^0
10^−3
10^−7
10^−10
0
128
255
mode number

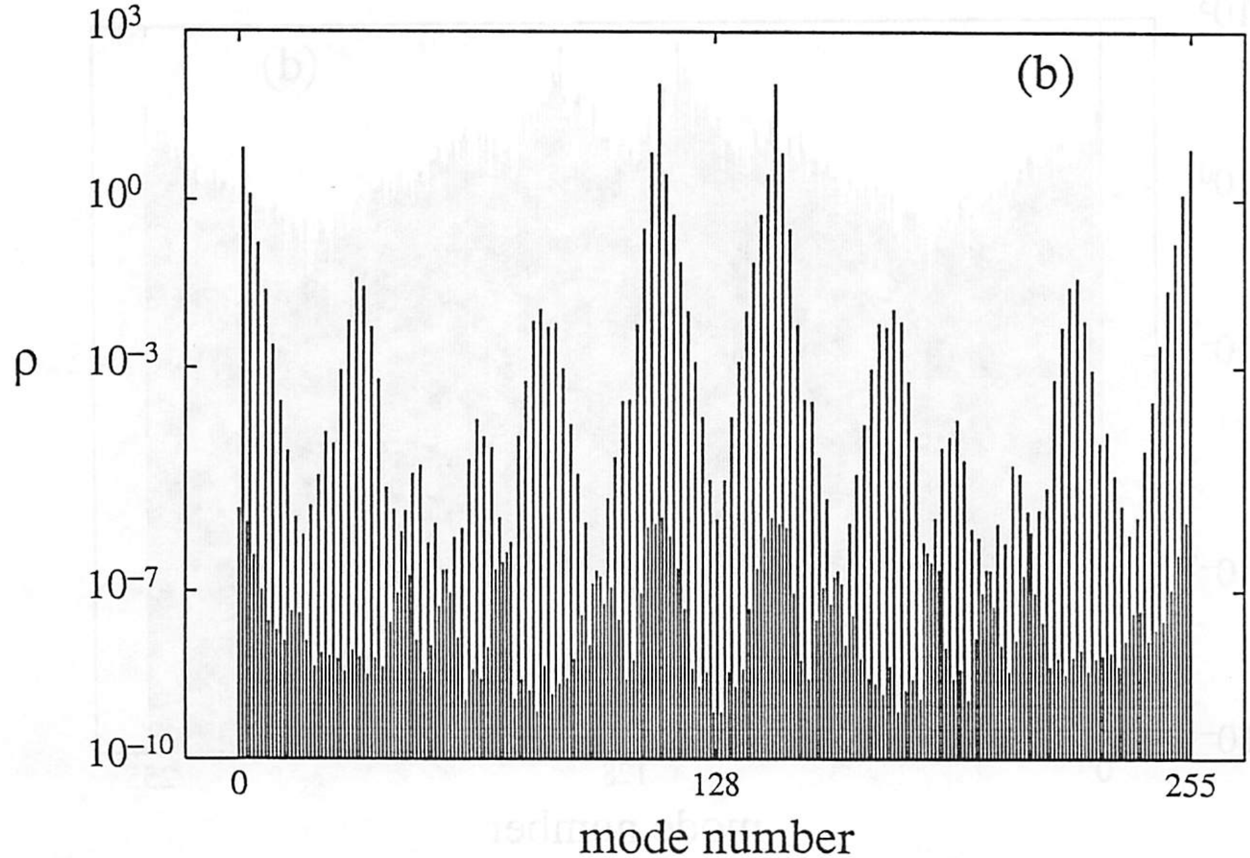

(b)
ρ
10^3
10^0
10^−3
10^−7
10^−10
0
128
255
mode number

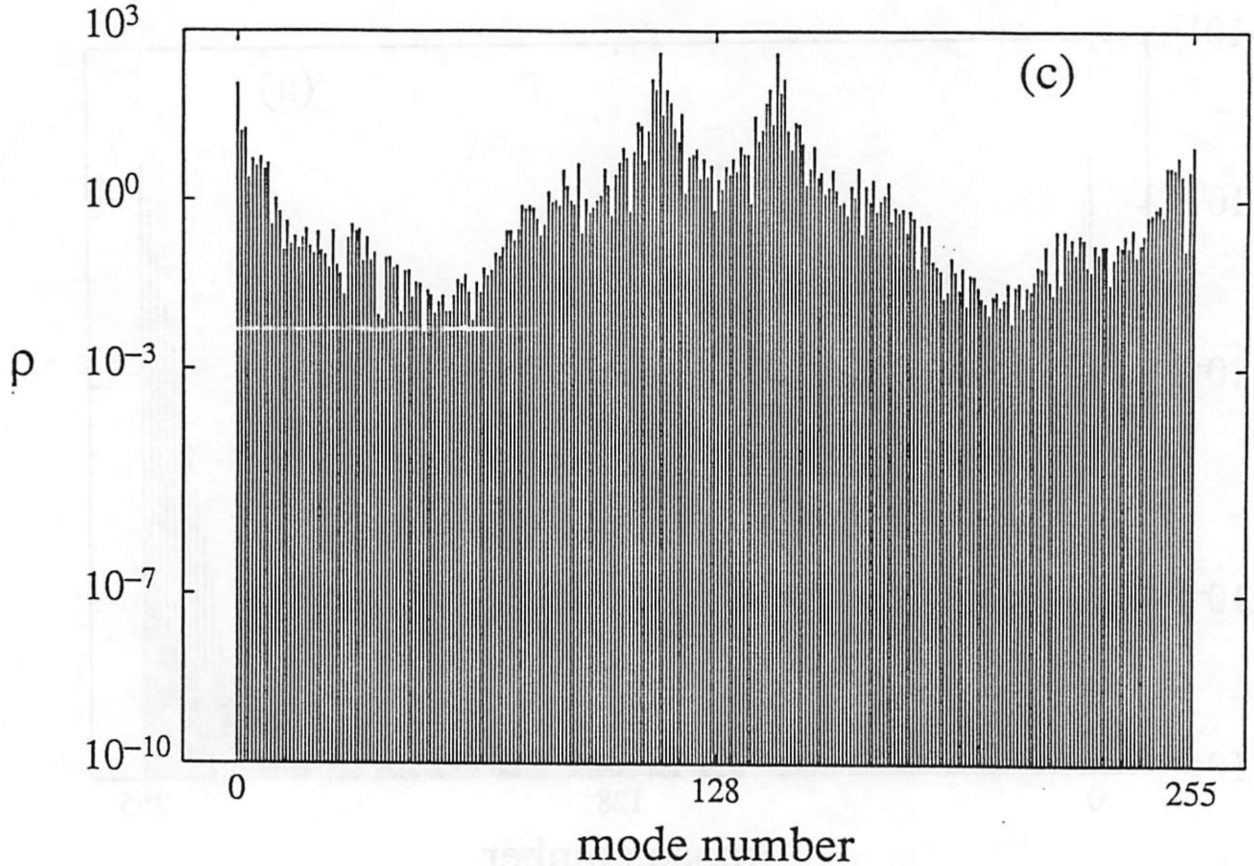
(c)
ρ
10^3
10^0
10^{-3}
10^{-7}
10^{-10}
0
128
255
mode number

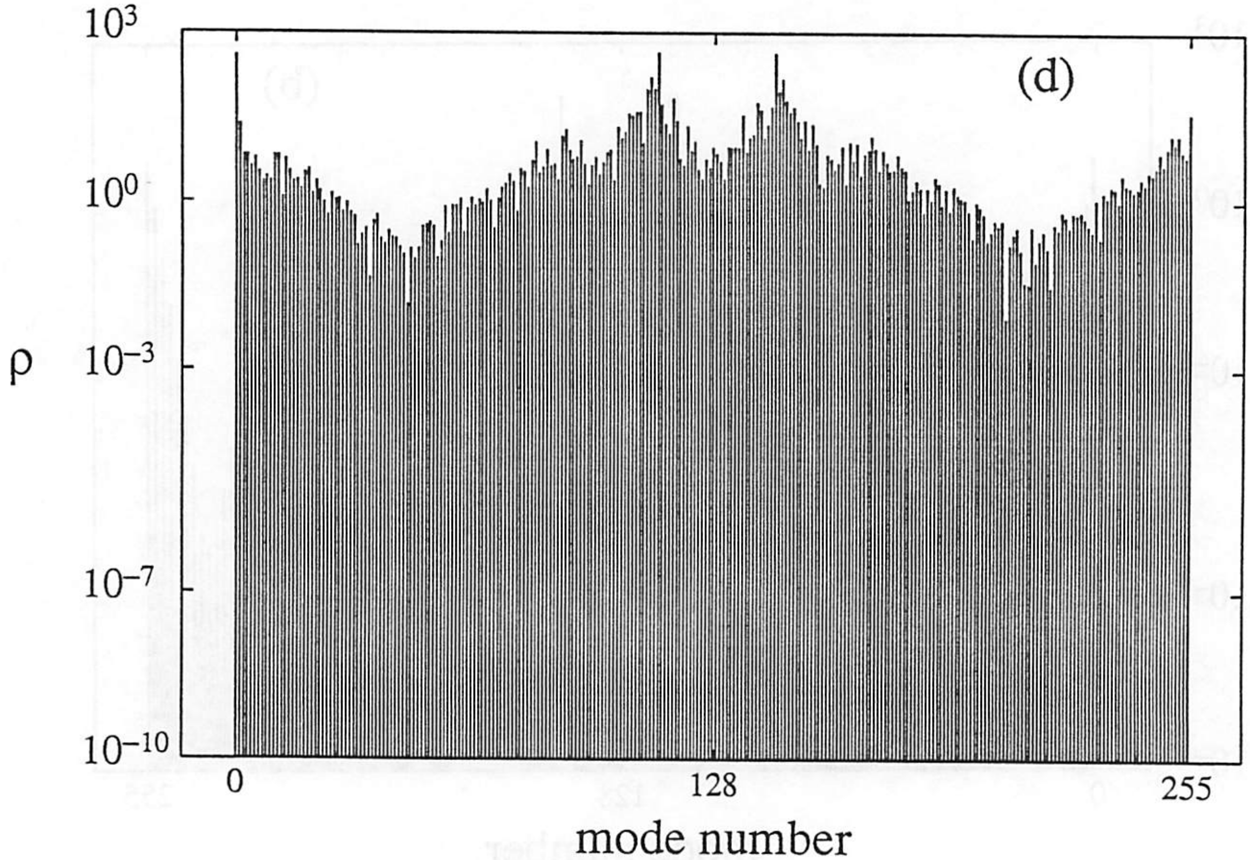
(d)
ρ
10^3
10^0
10^{-3}
10^{-7}
10^{-10}
0
128
255
mode number

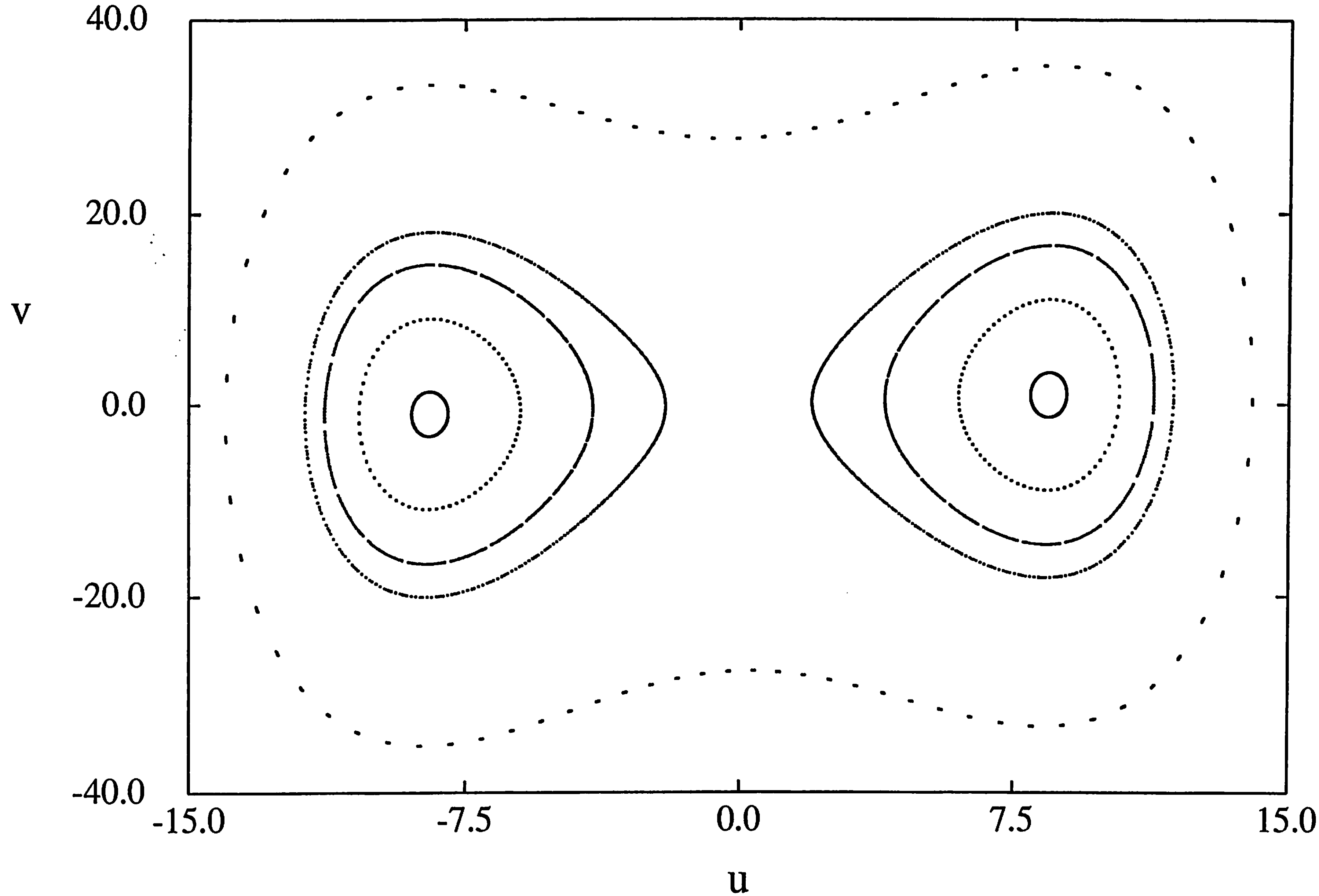
40.0
20.0
0.0
-20.0
-40.0
v
-15.0
-7.5
0.0
7.5
15.0
u

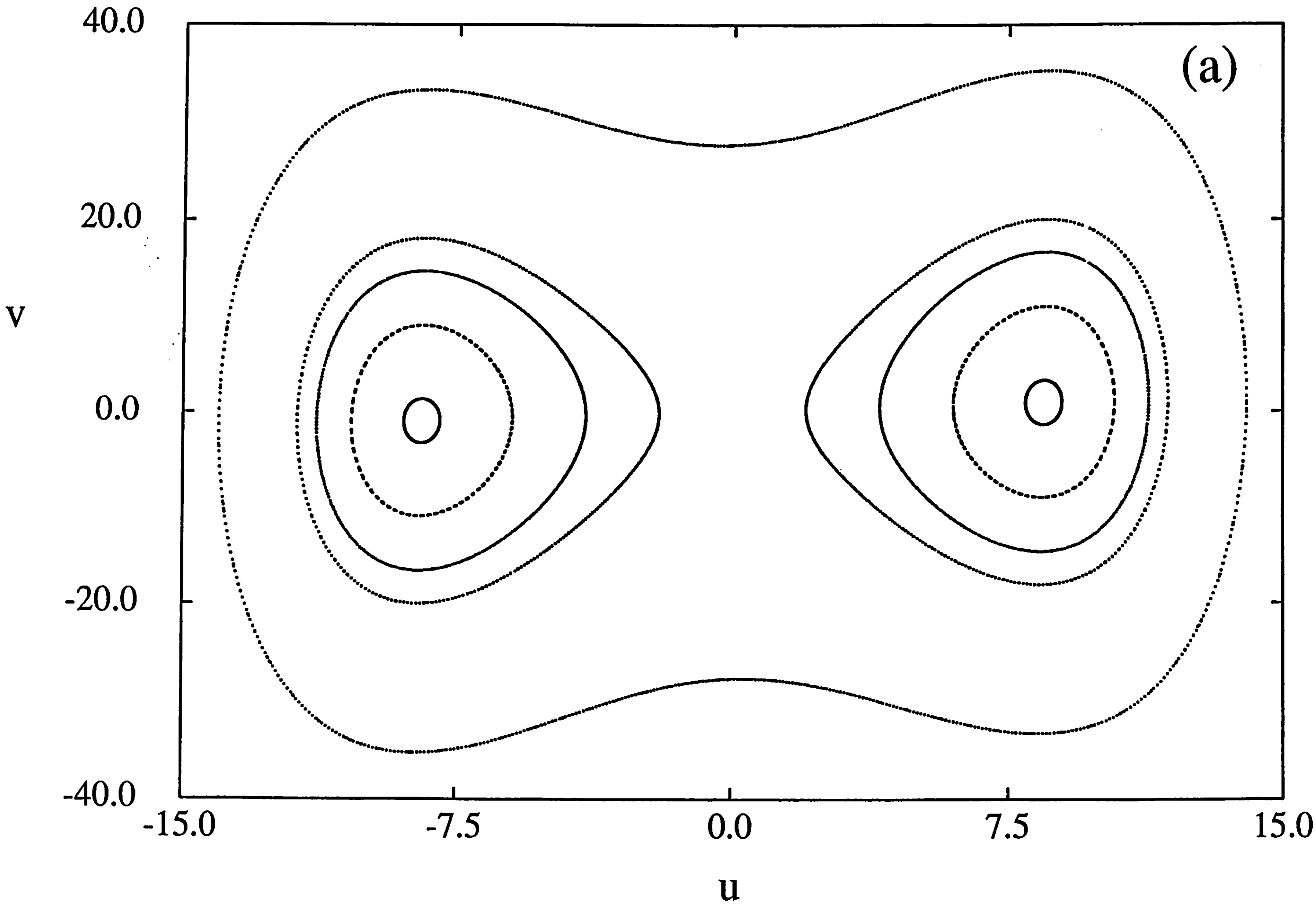

(a)
40.0
20.0
0.0
-20.0
-40.0
v
-15.0
-7.5
0.0
7.5
15.0
u

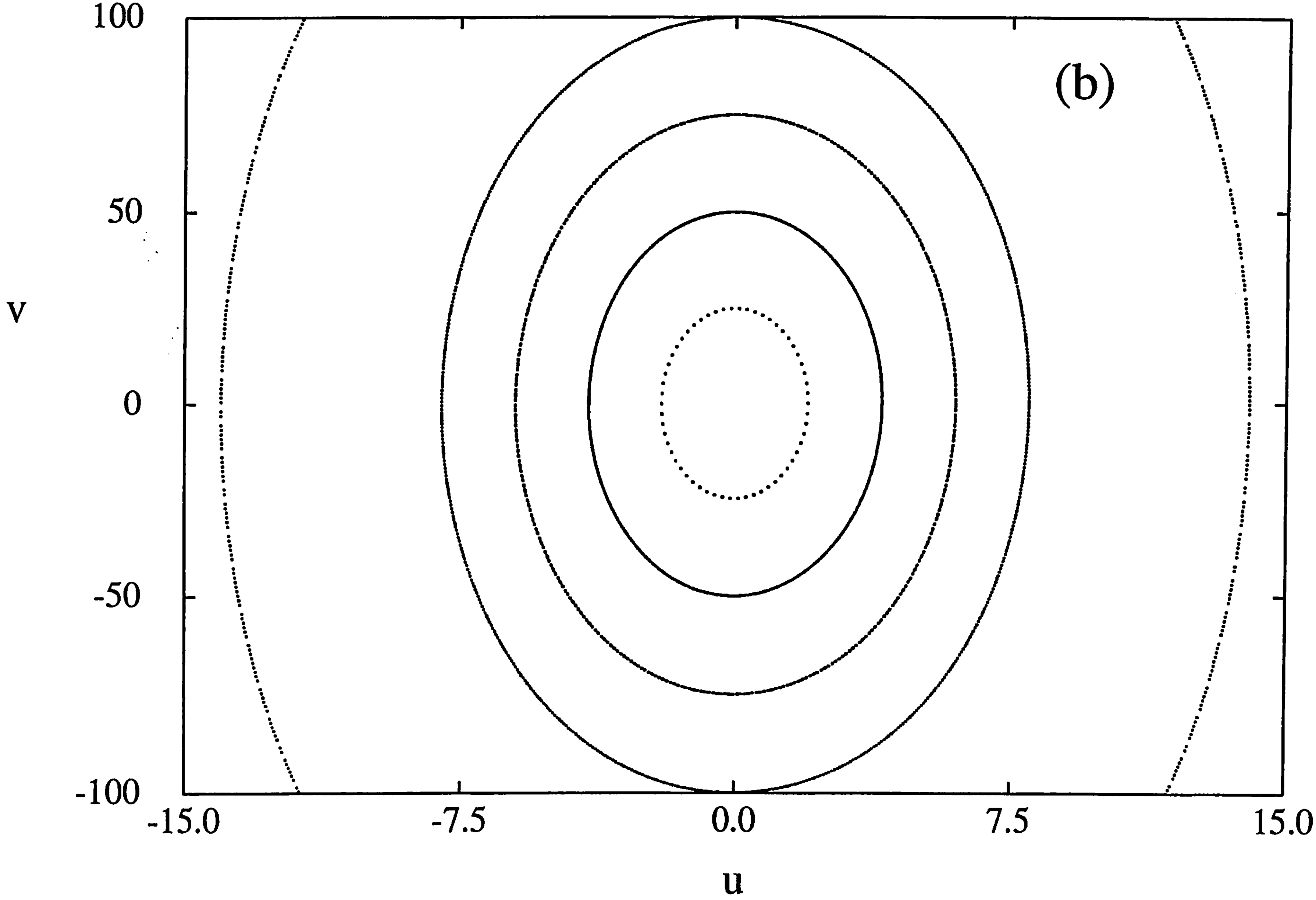
(b)
100
50
0
-50
-100
v
-15.0
-7.5
0.0
7.5
15.0
u

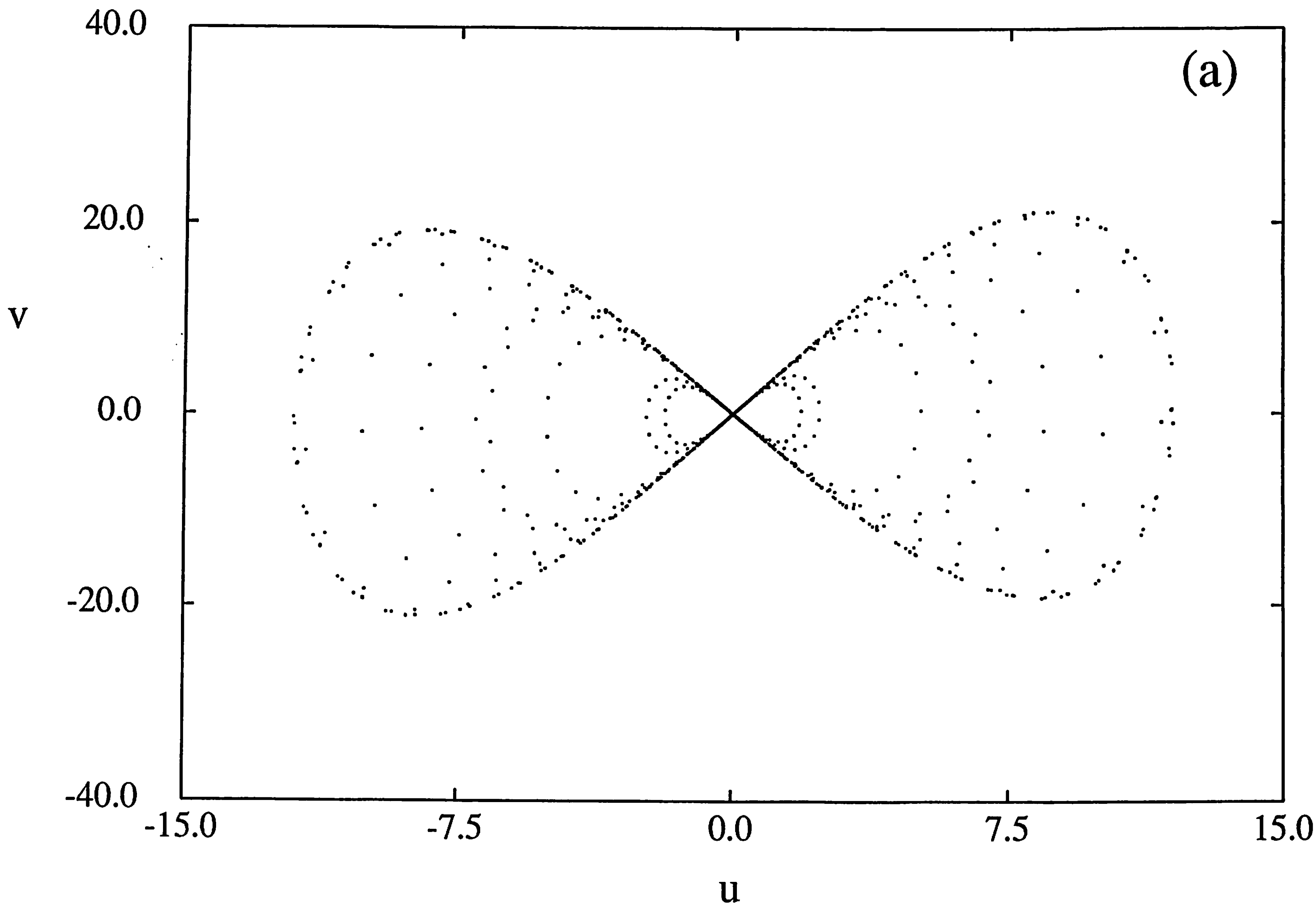

(a)
40.0
20.0
0.0
-20.0
-40.0
v
-15.0
-7.5
0.0
7.5
15.0
u

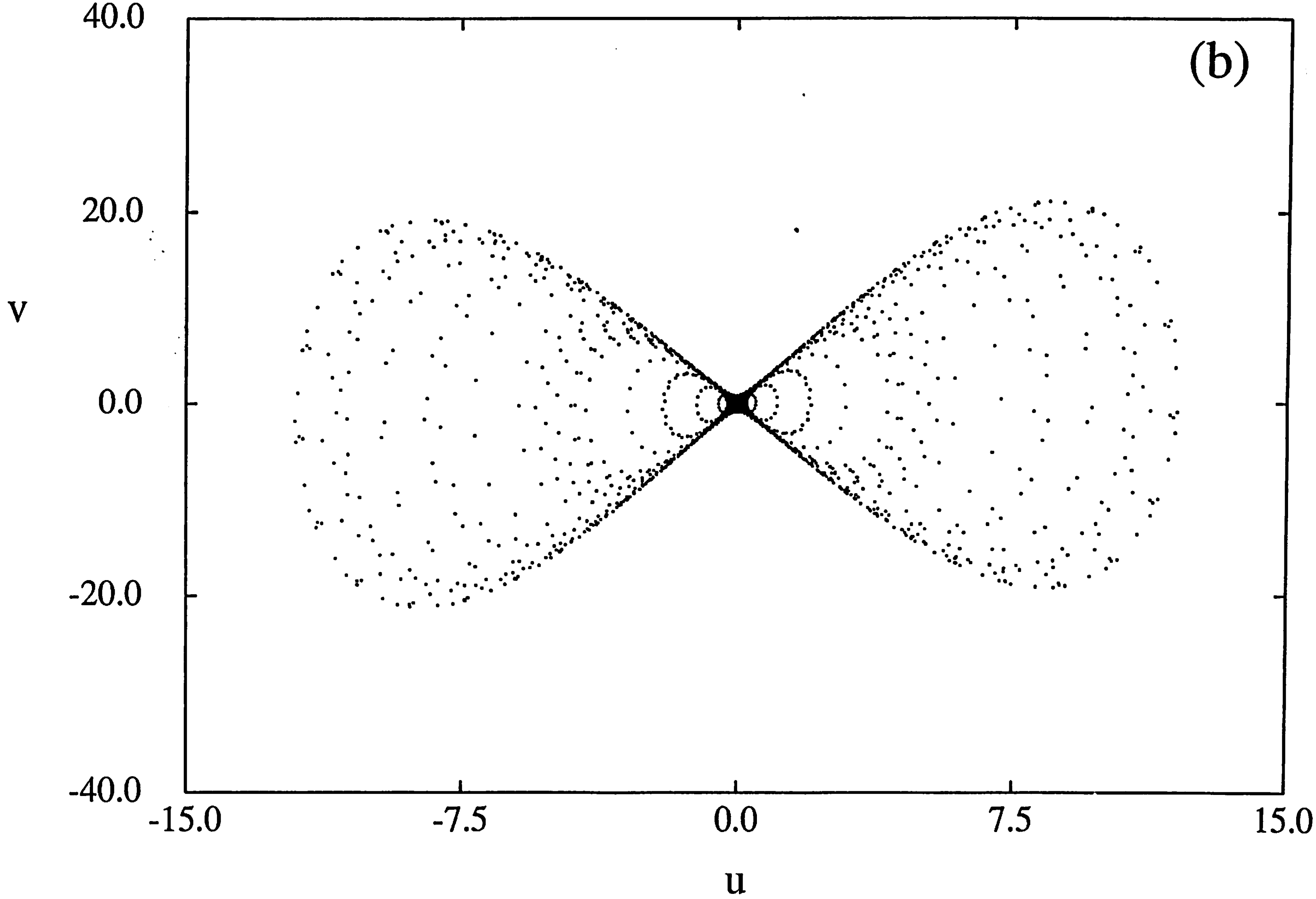
(b)
40.0
20.0
0.0
-20.0
-40.0
v
-15.0
-7.5
0.0
7.5
15.0
u